

- <sup>56</sup>V. F. Weisskopf and E. P. Wigner, *Z. Physik* **63**, 54 (1930); **65**, 18 (1930).
- <sup>57</sup>W. E. Lamb, Jr., *Phys. Rev.* **85**, 259 (1952).
- <sup>58</sup>F. E. Low, *Phys. Rev.* **88**, 53 (1952).
- <sup>59</sup>G. Källén, *Elementary Particle Physics* (Addison-Wesley, London, 1964), p. 375.
- <sup>60</sup>T. D. Lee and C. S. Wu, *Ann. Rev. Nucl. Sci.* **15**, 381 (1965).
- <sup>61</sup>W. E. Cleland, Ph.D. thesis, Yale University, 1964 (unpublished). Additional details on the experiment are given in this thesis.
- <sup>62</sup>The titanium sponge was Grade A1 obtained from E. I. du Pont de Nemours and Co.
- <sup>63</sup>Hewlett-Packard model No. 540 B.
- <sup>64</sup>Beckman model No. 7370 output meter and Model No. 7570 counter series.
- <sup>65</sup>Hewlett-Packard model No. 430 C.
- <sup>66</sup>Microwave Associates model No. MA 3459.
- <sup>67</sup>M. Bardon, P. Franzini, and J. Lee, *Phys. Rev.* **126**, 1826 (1962).
- <sup>68</sup>J. Rosen, Nevis Report No. 92, Columbia University (unpublished).
- <sup>69</sup>J. Bailey, W. Cleland, V. W. Hughes, R. Prepost, and K. Ziock, *Bull. Am. Phys. Soc.* **7**, 264 (1962).
- <sup>70</sup>R. M. Mobley, J. M. Bailey, W. E. Cleland, V. W. Hughes, and J. E. Rothberg, *J. Chem. Phys.* **44**, 4354 (1966); R. M. Mobley, J. J. Amato, V. W. Hughes, J. E. Rothberg, and P. A. Thompson, *ibid.* **47**, 3074 (1967); R. M. Mobley, J. M. Bailey, W. E. Cleland, V. W. Hughes, and J. E. Rothberg, in *Fourth International Conference on the Physics of Electronic and Atomic Collisions, Quebec*, 1965 (Science Bookcrafters, Hasting-on-Hudson, N. Y., 1965), p. 194.
- <sup>71</sup>S. Marder, V. W. Hughes, C. S. Wu, and W. R. Bennett, Jr., *Phys. Rev.* **103**, 1258 (1956); W. B. Teutsch and V. W. Hughes, *ibid.* **103**, 1266 (1956).
- <sup>72</sup>E. B. D. Lambe, *Polarization, Matière, et Rayonnement* (Société Française de Physique, Paris, 1969), p. 441.
- <sup>73</sup>N. F. Ramsey, *Nuclear Moments* (Wiley, New York, 1953).
- <sup>74</sup>R. A. Brown and F. M. Pipkin *Phys. Rev.* **174**, 48 (1968); F. M. Pipkin and R. H. Lambert, *ibid.* **127**, 787 (1962).

## Fine-Structure Measurement of Singly Ionized Helium, $n = 4^*$

Ralph R. Jacobs, † Kenneth R. Lea, and Willis E. Lamb, Jr.

*Yale University, New Haven, Connecticut 06520*

(Received 15 June 1970)

Precision measurements of the energy differences  $S_4(4^2S_{1/2} - 4^2P_{1/2})$  and  $\Delta E_4 - S_4(4^2P_{3/2} - 4^2S_{1/2})$  in  $(\text{He}^4)^+$  are reported. The experimental results,  $S_4 = 1768 \pm 5$  MHz and  $\Delta E_4 - S_4 = 20179.7 \pm 1.2$  MHz, agree with the values predicted by quantum electrodynamic theory,  $S_4 = 1768.34 \pm 0.51$  MHz and  $\Delta E_4 - S_4 = 20180.78 \pm 0.56$  MHz. An electron gun excites the states of interest in a section of waveguide containing helium gas. A magnetic field applied perpendicular to the waveguide axis is used to scan a microwave resonance between suitable Zeeman levels for a fixed frequency of oscillating electric field in the waveguide. Any induced electric dipole transitions  $4^2S_{1/2} \rightarrow 4^2P_{1/2}$  or  $4^2S_{1/2} \rightarrow 4^2P_{3/2}$  reduce the intensity of 1215-Å radiation which is emitted in the natural decay of  $4S$  to  $2P$ . This light is directed onto an ultraviolet-detecting phototube whose output is measured by a lock-in detector for which the synchronous signal is provided by square-wave amplitude modulation of the microwave field. The resonances obtained by varying the magnetic field are fitted to a theoretical line-shape formula by a computerized least-squares program. The resulting best-fit parameters include either  $S_4$  or  $\Delta E_4 - S_4$ , depending on the transition studied. Consideration is given to the dependence of the resonance center on the gun current, helium pressure, and microwave power level.

### I. BASIS OF THE EXPERIMENT

#### A. Introduction

The fine structure of one-electron atoms has been the subject for much experimental and theoretical investigation since 1947, when Lamb and Retherford<sup>1</sup> discovered that, contrary to the Dirac theory, the states  $2^2S_{1/2}$  and  $2^2P_{1/2}$  in hydrogen were non-degenerate. In addition to the "Lamb shift"  $S_n$  (interval between  $n^2S_{1/2}$  and  $n^2P_{1/2}$ ), another important energy separation  $\Delta E_n = n^2P_{3/2} - n^2P_{1/2}$  can be determined, which yields a value for the fine-structure constant  $\alpha$ , the expansion parameter in quan-

tum-electrodynamic (QED) theory.<sup>2,3</sup> In the case of hydrogen, disagreements have existed among different experiments and between experiment and theory on the value of  $S_2$  as well as among various experimental results for the value of  $\Delta E_2$ . The present research was undertaken with the ultimate hope that fine-structure measurements in the  $n = 4$  term of singly ionized helium would remove some of the difficulties surrounding the value of  $S_2$  in H by limiting the coefficients of certain uncalculated  $n$ - and  $Z$ -dependent QED terms, and perhaps, through the value of  $\Delta E_4$ , provide another competitive determination of  $\alpha$ . This paper reports the

most accurate measurements to date of

$$s_4 = 4^2S_{1/2} - 4^2P_{1/2}$$

and

$$\Delta E_4 - s_4 = 4^2P_{3/2} - 4^2S_{1/2}$$

in singly ionized He<sup>+</sup>. For reasons given later, the error limits are not small enough to establish the value of  $s_4$  in He<sup>+</sup> to less than the uncertainty in its theoretical calculation or to support a particular value of  $\alpha$  determined from other investigations. However, the results do confirm, to the stated accuracy, the correctness of quantum-electrodynamic theory in the case of hydrogenic systems for which  $Z = 2$  and  $n = 4$ .<sup>2,3</sup> Since the completion of the present work, Appelquist and Brodsky<sup>3</sup> have reported a new calculation of  $s_n$  which substantially eliminates the disagreement between experiment and theory in hydrogen.

Several experimenters have studied the He<sup>+</sup>,  $n = 4$  fine structure. Included among the recent optical spectroscopic studies are those of Series,<sup>4</sup> Herzberg,<sup>5</sup> Roesler and DeNoyer,<sup>6</sup> Roesler and Mack,<sup>7</sup> and Larson and Stanely.<sup>8</sup> Microwave spectroscopic techniques were employed by Hatfield and Hughes,<sup>9</sup> Beyer and Kleinpoppen,<sup>10</sup> and Lea, Leventhal, and Lamb,<sup>11</sup> while Eck and Huff<sup>12</sup> observed "anticrossings" in optical resonance fluorescence. Recently, Hadeishi<sup>13</sup> reported the observation of the Lamb shift by the detection of quantum beats, due to coherent electron-impact excitation of  $S$ - and  $P$ -state Zeeman sublevels, in transitions from  $n = 4$  to  $n = 3$ .

Unfortunately, the results of the optical measurements, which utilized the 4686-Å transition between  $n = 4$  and  $n = 3$  in He<sup>+</sup>, have suffered from Doppler broadening. Series reported a shift of the  $4^2P_{1/2}$  level an order of magnitude greater than that predicted by theory, but this deviation was not confirmed in the later work of Herzberg. As determined by Roesler and DeNoyer and Roesler and Mack, differential Doppler displacements of the various optical lines originating from the  $n = 4$  fine-structure levels could explain many of the spectroscopic anomalies. Larson and Stanley used an atomic-beam source instead of the cryogenically cooled hollow-cathode discharge of Roesler and Mack. This offered the possibility of greatly reduced Doppler widths, but there was still an appreciable width due to recoil from the electron-bombardment excitation. Even in these two latest optical measurements, the experimental precision did not allow for testing the quantum-electrodynamical level shift theory to better than a few percent.

Series and Fox,<sup>14</sup> using a gas discharge as a source of excited helium ions, were unsuccessful in finding any microwave transitions between the  $4^2S_{1/2}$  and  $4^2P_{1/2}$  levels. However, electron-impact

collisions that simultaneously ionize and excite helium atoms to the He<sup>+</sup>,  $n = 4$  levels were successfully employed in three microwave-optical experiments. Beyer and Kleinpoppen, Hatfield and Hughes, and Lea, Leventhal, and Lamb used electric dipole transitions to create population changes of the  $4S$  and  $4P$  levels which subsequently altered the intensity of 4686-Å decay radiation in the first two cases and 1215-Å decay radiation in the third. The work of Eck and Huff concentrated on signals associated with three crossings of  $S$  with  $F$  levels. Unexplained systematic effects have thus far prevented them from making precision measurements of the fine-structure separations. The published efforts of Hadeishi were not intended to serve as precision measurements, but, rather, tested certain features of a proposal by Series<sup>15</sup> for determining the energy interval between atomic states of different parity.

In the present experiment, an electron beam passes through a section of waveguide containing helium at a pressure of approximately  $10^{-2}$  Torr. For appropriate electron energies, a simultaneous process of ionization and excitation of some atoms to the He<sup>+</sup>,  $n = 4$  states results. Because the output power of microwave oscillators is very frequency dependent, a fixed microwave (rf) frequency is established in the waveguide, and a variable external magnetic field is utilized to bring a pair of fine-structure Zeeman sublevels into resonance. These  $4^2S_{1/2} - 4^2P_{1/2}$  or  $4^2S_{1/2} - 4^2P_{3/2}$  electric dipole transitions diminish the intensity of 1215-Å radiation emitted in the spontaneous decay of  $4S$  to  $2P$ . This radiation leaves the experimental region, which is located at one focus of an ellipsoidal-mirror light pipe, through holes in the waveguide and is directed toward a nitric-oxide-filled ultraviolet detector situated at the second focus. Following the gas cell is a lock-in (phase-sensitive) detector whose reference signal is supplied by a source which also controls the amplitude modulation of the rf field. The output of this detector along with other experimental information is forwarded to a data-recording system. Variation of the magnetic field over appropriate ranges produces the experimental resonance. The resonance data, which are a record of the intensity of the rf-altered decay radiation as a function of the magnetic field, are then fitted by a computerized least-squares program containing a line-shape formula which has, among the parameters yielding the final fit, either  $s_4$  or  $\Delta E_4 - s_4$ .

The basis for the experiment is given in Fig. 1, which depicts the energy levels of He<sup>+</sup> up to and including  $n = 4$ . With the rf off, i. e., when no electric dipole coupling of the  $4S$  and  $4P$  levels exists, the states initially excited by electron impact decay spontaneously with characteristic lifetimes<sup>16</sup> to lower levels. Only certain decay routes are shown in the figure. Population differences arise among

the  $S$ ,  $P$ ,  $D$ , and  $F$  sublevels in  $n=4$  because of the unequal excitation rates and different lifetimes. Fifty-eight percent of the  $4S$  states decay to  $2P$ , then to  $1S$ , emitting successively  $1215\text{-}\text{\AA}$  and  $304\text{-}\text{\AA}$  radiation. The less populated  $4P$  levels decay primarily (84%) to  $1S$  with the emission of  $243\text{-}\text{\AA}$  radiation. When the microwave field is on, the induced transitions cause a readjustment in the populations of the  $4S$  and  $4P$  states resulting in a decrease of  $1215\text{-}\text{\AA}$  and  $304\text{-}\text{\AA}$  light with a corresponding increase in the intensity of the  $243\text{-}\text{\AA}$  line. Since the detection system is optically narrow-banded between approximately  $1180$  and  $1343\text{ \AA}$ , only the  $1215\text{-}\text{\AA}$  intensity changes are recorded.

### B. Line Shape

The theory presented in this section was given by Lamb and Sanders<sup>17</sup> and is included for completeness. A theoretical line shape describing the experimental resonances is derived by first considering an atom with two excited sublevels  $S$  and  $P$  which have lifetimes for radiative decay to lower states  $\tau_S = 1/\gamma_S$  and  $\tau_P = 1/\gamma_P$ . One introduces electron-excitation rates  $r_S$  and  $r_P$  to the  $\text{He}^+$ ,  $n=4$ ,  $S$  and  $P$  states. Differential equations that describe the excited state populations are

$$\begin{aligned} \dot{n}_S &= r_S - \gamma_S n_S + W(n_P - n_S), \\ \dot{n}_P &= r_P - \gamma_P n_P + W(n_S - n_P), \end{aligned} \quad (1)$$

where  $W$  represents the rate of rf-induced transitions. Because of the steady-state character of the experiment, we have  $\dot{n}_S = 0$  and  $\dot{n}_P = 0$ . Solving Eqs. (1) for this condition, one obtains the steady-state populations

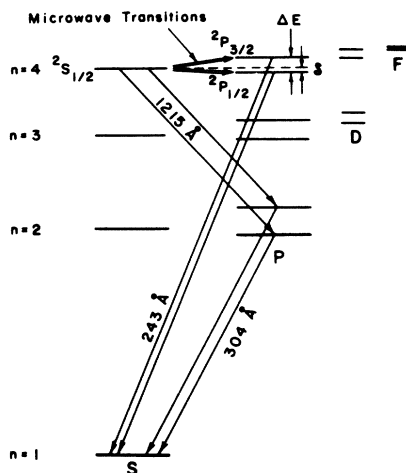


FIG. 1. Energy levels for singly ionized helium up through  $n=4$ . Note that the diagram is not drawn to scale and that only the optical decays mentioned in the text are shown.

$$\begin{aligned} n_S &= [r_S \gamma_P + W(r_S + r_P)] / [\gamma_S \gamma_P + W(\gamma_S + \gamma_P)], \\ n_P &= [r_P \gamma_S + W(r_S + r_P)] / [\gamma_S \gamma_P + W(\gamma_S + \gamma_P)]. \end{aligned}$$

An expression for the rate of emission of photons that are detected in the experiment is

$$r(W) = f_S \gamma_S n_S + f_P \gamma_P n_P,$$

where  $f_S$  and  $f_P$  represent those fractions of the total decays from the excited  $4S$  and  $4P$  states that yield detectable ultraviolet quanta. The lock-in signal, i. e., the intensity with rf on minus that with rf off, is

$$S = r(W) - r(0) = \frac{-(f_S - f_P)(r_S/\gamma_S - r_P/\gamma_P)W}{1 + [W(\gamma_S + \gamma_P)/\gamma_S \gamma_P]}.$$

The expression for the rate  $W$  is obtained from a statistical density-matrix treatment of the problem. Under certain assumptions it can be shown<sup>17,18</sup> that

$$W = \frac{1}{4}(\gamma_S + \gamma_P) |V|^2 / [(\nu - \omega)^2 + \frac{1}{4}(\gamma_S + \gamma_P)^2], \quad (2)$$

in which  $\nu$  is the rf circular frequency and  $\omega$  the resonant circular frequency. The quantity  $\hbar V$  is the matrix element between the  $S$  and  $P$  states of the time-independent amplitude of the interaction energy between the atom and the rf field. Specifically, we have  $\hbar V = \langle P | e \vec{E} \cdot \vec{r} | S \rangle$ , where the microwave field  $\vec{E}_{\text{rf}}(t) = \vec{E} \cos \nu t$ . Substitution of this value for  $W$  into the expression for the lock-in signal yields

$$S = \frac{-(f_S - f_P)(r_S/\gamma_S - r_P/\gamma_P)(\gamma_S + \gamma_P)^{1/4} |V|^2}{(\omega - \nu)^2 + \frac{1}{4}(\gamma_S + \gamma_P)^2 + \frac{1}{4}[(\gamma_S + \gamma_P)^2/\gamma_S \gamma_P] |V|^2}. \quad (3)$$

This treatment can be straightforwardly extended to the situation in which a third nearby level is electrostatically coupled to one of the primary two.<sup>18</sup> Such an extension of the line-shape theory would be necessary to analyze the  $S$  to  $D$  resonance described in Sec. III A.

### C. Zeeman Effect and Working Hamiltonian

The Zeeman effect of one-electron atoms has been extensively treated elsewhere.<sup>17,19</sup> The effective Hamiltonians for the states of interest in singly ionized helium are

$$\mathcal{H}_S = s + g_S \mu_0 \vec{S} \cdot \vec{H} \quad \text{for } 4S \text{ states,}$$

$$\mathcal{H}_P = \frac{2}{3} \Delta E (1 + \vec{L} \cdot \vec{S}) + g_S \mu_0 \vec{S} \cdot \vec{H} + g_L \mu_0 \vec{L} \cdot \vec{H} \quad \text{for } 4P \text{ states,}$$

$$\mathcal{H}_D = \Delta E + \Sigma + \frac{2}{3} \mathcal{D} E (\frac{3}{2} + \vec{L} \cdot \vec{S}) + g_S \mu_0 \vec{S} \cdot \vec{H} + g_L \mu_0 \vec{L} \cdot \vec{H} \quad \text{for } 4D \text{ states,}$$

$$\begin{aligned} \mathcal{H}_F &= \Delta E + \Sigma + \mathcal{D} E + \mathcal{C} + \frac{2}{7} \mathcal{D} E (2 + \vec{L} \cdot \vec{S}) \\ &+ g_S \mu_0 \vec{S} \cdot \vec{H} + g_L \mu_0 \vec{L} \cdot \vec{H} \quad \text{for } 4F \text{ states,} \end{aligned}$$

where the zero of energy is taken to be that of the

4<sup>2</sup>P<sub>1/2</sub> states at zero magnetic field. Note that for the discussion in this section only, the subscript "4" has been omitted from the symbols for the level shifts and doublet separations. In Fig. 2 are shown the zero-magnetic-field-energy separations. Table I lists the values of these zero field energies and other constants appearing in the Hamiltonians.

A computer was used to calculate the transition frequencies, dipole matrix elements, and Stark shifts for the 32 magnetic sublevels of He<sup>+</sup>, n = 4. An energy matrix was obtained by evaluating the previous Hamiltonians in the  $Lm_LSm_S$  ("high field") representation. This matrix was then diagonalized at each working magnetic field value by a computer program based on an iterative technique due to Jacobi.<sup>20</sup> The transition frequencies were derived from the eigenvalues by subtracting appropriate pairs. The electric dipole matrix elements were computed using the eigenvectors provided by the diagonalization. Figure 3 shows the S- and P-state energy levels as a function of the magnetic field, while Fig. 4 shows the allowed dipole-transition frequencies as a function of the field.

#### D. Size of Expected Signals

In this section, we calculate (a) the size of the rf-induced signal as a percentage of the total light intensity given off in the n = 4 to n = 2 decays, (b) the value of the total light signal under typical experimental conditions, and (c) expected signal-to-noise (S/N) ratios.

The rate of emission of H<sub>β</sub> quanta (Balmer β radiation) from all n = 4 levels is given by

$$r(0) = 2r_S f_S + 6r_P f_P + 10r_D f_D + 14r_F f_F, \quad (4)$$

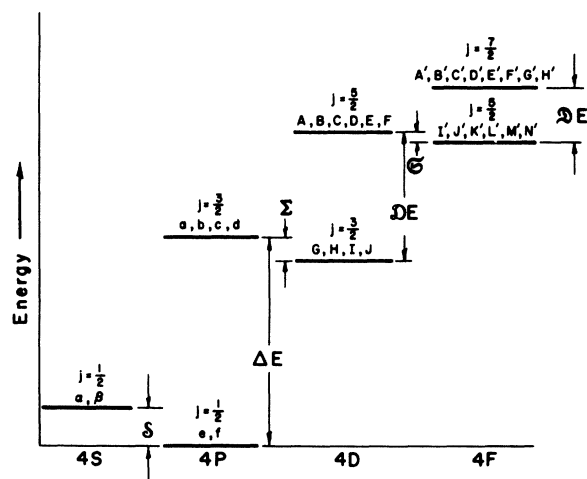


FIG. 2. n = 4 energy levels of singly ionized helium at zero magnetic field. For each fine-structure level, the various magnetic sublevels (in order of decreasing magnetic quantum number  $m_J$ ) are designated in the customary notation. The diagram is not drawn to scale.

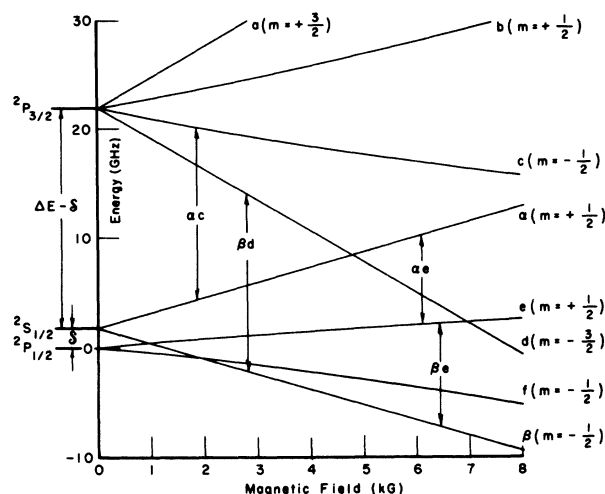


FIG. 3. Zeeman levels for 4S and 4P in He<sup>+</sup>. The transitions used for precision measurements are indicated by arrows. The labeling of the states follows the earlier notation of Lamb as in Ref. 19. Note that the 4D and 4F levels are not included.

where the quantities  $f_S$ ,  $f_P$ ,  $f_D$ , and  $f_F$  are the branching ratios for obtaining H<sub>β</sub> light from the 4S, 4P, 4D, and 4F levels, respectively, and  $r_S$ ,  $r_P$ ,  $r_D$ , and  $r_F$  represent the excitation rates to the corresponding individual Zeeman sublevels, each of

TABLE I. Values of constants used in the Hamiltonians.

Symbol	Value
$\mathcal{S}$	1768.34 ± 0.51 MHz <sup>a</sup>
$\Delta E$	21949.12 ± 0.09 MHz <sup>a</sup>
$\Sigma$	36.87 MHz <sup>b</sup>
$\mathcal{D}E$	7315.44 MHz <sup>b</sup>
$\mathcal{C}$	13.86 MHz <sup>b</sup>
$\mathcal{D}'E$	3657.63 MHz <sup>b</sup>
$g_S$	2.0023192 <sup>c</sup>
$g_L$	0.999864 <sup>d</sup>

<sup>a</sup>Values taken from Ref. 2, which used the value  $\alpha^{-1} = 137.03602(21)$  to calculate  $\mathcal{S}$  and  $\Delta E$ . A revised theoretical result  $\mathcal{S} = 1769.0 \pm 0.6$  MHz has recently been reported by T. Appelquist and S. J. Brodsky, Phys. Rev. Letters **24**, 562 (1970).

<sup>b</sup>Level shifts  $\Sigma$  and  $\mathcal{C}$  were calculated using results contained in J. M. Harriman, Phys. Rev. **101**, 594 (1956), while  $\mathcal{D}E$  and  $\mathcal{D}'E$  were determined using Eq. 21.5 in H. A. Bethe and E. E. Salpeter, *Quantum Mechanics of One and Two-Electron Atoms* (Springer-Verlag, Berlin, 1957), pp. 248-278, incorporating the indicated corrections.

<sup>c</sup>D. T. Wilkinson and H. R. Crane, Phys. Rev. **130**, 852 (1963). The correction to this value given by A. Rich, Phys. Rev. Letters **20**, 967 (1968) has a negligible effect on the present experiment.

<sup>d</sup>This value contains a correction due to the motion of the nucleus and is discussed further in Sec. IV F.

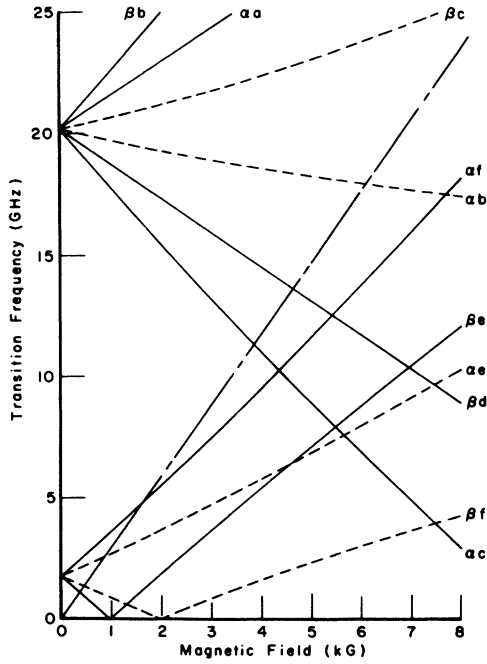


FIG. 4. Electric dipole ( $\Delta L = \pm 1$ ) transition frequency diagram for  $\text{He}^+$ ,  $n=4$ . The  $\sigma$ -type transitions (solid lines) are those in which  $\Delta m_L = \pm 1$ , whereas the  $\pi$ -type transitions (dashed lines) are those in which  $\Delta m_L = 0$ . The broken line represents the electron cyclotron frequency. As in Fig. 3, contributions by the  $4D$  and  $4F$  levels are not included.

which is assumed to be independent of  $m_J$ . The relative rates of excitation  $r_P/r_S$ ,  $r_D/r_S$ , and  $r_F/r_S$  can be determined from a knowledge of the total cross sections for excitation  $\sigma_S$ ,  $\sigma_P$ ,  $\sigma_D$ , and  $\sigma_F$ . An order of magnitude calculation using the sudden-approximation method<sup>21</sup> gives the following results for a bombarding voltage of 400 V:

$$\sigma_S = 14 \times 10^{-21} \text{ cm}^2, \quad \sigma_P = 5.9 \times 10^{-21} \text{ cm}^2,$$

$$\sigma_D = 0.079 \times 10^{-21} \text{ cm}^2, \quad \sigma_F = 0.0010 \times 10^{-21} \text{ cm}^2.$$

The values for the branching ratios are  $f_S = 0.5842$ ,  $f_P = 0.1190$ ,  $f_D = 0.7455$ , and  $f_F = 0.0$ .<sup>22</sup> Noting that the relative rates of excitation  $r_P/r_S$ ,  $r_D/r_S$ , and  $r_F/r_S$  are given by  $\frac{1}{3}(\sigma_P/\sigma_S)$ ,  $\frac{1}{5}(\sigma_D/\sigma_S)$ , and  $\frac{1}{7}(\sigma_F/\sigma_S)$ , respectively, Eq. (4) can be rewritten as

$$r(0) = r_S [2f_S + 6f_P(0.14) + 10f_D(1.1 \times 10^{-3})] = 1.3r_S.$$

When an appropriate rf field is turned on, transitions between two sublevels  $S$  and  $P$  can occur. We now consider the signal  $S = r(W) - r(0)$  as defined in Eq. (3) for large rf fields, i. e., large enough to produce 100% saturation of the two-level resonance. In this limit of very large  $W$ , we obtain from Eq. (3)

$$S = - (f_S - f_P) \left( \frac{\gamma_S}{\gamma_S} - \frac{\gamma_P}{\gamma_P} \right) \frac{\gamma_S \gamma_P}{\gamma_S + \gamma_P}.$$

Substituting for the quantities in the above equation and assuming  $r_S/\gamma_S \gg r_P/\gamma_P$ , we obtain

$$S = -0.44r_S = -0.34r(0).$$

Thus, application of a very large rf electric field can cause a 34% reduction in the total amount of  $H_\beta$  light at the detector according to the results of the sudden-approximation model for the total cross sections of excitation. The  $\alpha c$  resonance at 16 GHz was arbitrarily selected to measure the magnitude of the rf saturated signal in terms of a fraction of the total Balmer  $\beta$  intensity. The resonance maximum represented a 2.4% change of the  $H_\beta$  intensity for the chosen rf power level. From the width of this resonance, it was inferred that this signal represented 14% of its saturated height. Thus, the maximum fraction of the total light which was available for use as a signal was 17%, a factor of 2 less than the 34% predicted. This discrepancy is not considered serious because of the approximate nature of the calculation. For example, if the relative rates of excitation to the various  $n=4$  sublevels were taken to be unity rather than proportional to the ratios of the cross sections divided by the statistical weights, then the saturated signal should be only 5% of the background.

We now calculate the total light intensity expected from all the  $n=4$  levels with no rf. If  $I$  represents the bombarding electron current,  $n$  the number density of helium atoms, and  $l$  the length of the interaction space, then one can write for the rate  $r(0)$  of  $H_\beta$  quanta emitted from all the  $n=4$  levels the expression

$$r(0) = (f_S \sigma_S + f_P \sigma_P + f_D \sigma_D + f_F \sigma_F) n l (I/e). \quad (5)$$

Typical experimental conditions were

$$I/e = 9.4 \times 10^{15} \text{ sec}^{-1} (1.5 \text{ mA}),$$

$$n = 3.3 \times 10^{14} \text{ cm}^{-3} (9.2 \times 10^{-3} \text{ Torr pressure at } 20^\circ \text{C}),$$

$$l = 1.1 \text{ cm}.$$

Substitution of these quantities and the previously assigned values for the branching ratios and excitation cross sections into Eq. (5) yields

$$r(0) = 3.0 \times 10^{10} \text{ sec}^{-1}.$$

If one lets  $\eta$  be the fraction of light from the interaction region impinging on the NO detector and  $Q$  its quantum efficiency, then the expression for the total photocurrent  $S_{\text{TPC}}$  is  $S_{\text{TPC}} = r(0)\eta Qe$ . Letting  $\eta = 0.0068$  and  $Q = 0.35$ , this expression becomes  $S_{\text{TPC}} = 1.2 \times 10^{-11} \text{ A}$ , whereas a measurement gave,  $S_{\text{TPC}}(\text{observed}) = 1.8 \times 10^{-11} \text{ A}$ . Thus the expected total photocurrent is about 30% less than that observed. Such a discrepancy is easily accounted for by the uncertainties in the values assigned to the various quantities of Eq. (5).

If one assumes that the principal sources of noise

in the experiment were due to shot noise at the nitric oxide (NO) cell and Johnson noise developed across the feedback resistor  $R_F$  in the preamplifier (see Sec. II C), then a value for the expected signal-to-noise ( $S/N$ ) ratio under typical experimental conditions can be readily obtained. An expression for the rate of photoelectrons ( $r_e$ ) leaving the NO cell with the rf off is  $r_e = \eta Q r(0) = 0.71 \times 10^8 \text{ sec}^{-1}$ .

Assuming that the resonance causes a change  $\kappa$  in the total  $H_\beta$  radiation, then the change in this rate,  $S$ , with the rf on becomes  $S = \kappa \eta Q r(0)$ . If this NO-cell current is now averaged for a time  $\tau$  (sec), then the statistical fluctuation of the signal is  $(r_e \tau)^{1/2}$ . The expression for the rms Johnson noise current is  $(4kT\Delta f/R)^{1/2}$ , where  $k$  is Boltzmann's constant,  $T$  is the absolute temperature of the resistor  $R$ , and  $\Delta f$  is the frequency bandwidth. Adding the Johnson noise in quadrature to the shot noise yields the signal-to-noise expression

$$S/N = \frac{\kappa \eta Q r(0) \tau^{1/2}}{\sqrt{2} [\eta Q r(0) + 4kT/R\tau]^{1/2}} \quad (6)$$

The factor  $\sqrt{2}$  accounts for the fact that the signal  $S$  is the difference between two signals, one with rf on, the other with rf off, each of which contributes to the noise. For a comparison with the observed  $S/N$  ratio, the relevant quantities had the following values:  $\eta Q r(0)$  as previously given,  $\kappa = 0.024$ ,  $\tau = 100 \text{ sec}$ ,  $R = 10^{10} \Omega$ , and  $T = 300 \text{ }^\circ\text{K}$ . The  $S/N$  ratio predicted by Eq. (6) is  $S/N = 1035$ , whereas ten successive lock-in readings of the  $\alpha c$  resonance center gave  $S/N = 1150$ .

## II. APPARATUS

### A. Introduction

The present experimental arrangement differs markedly from the original Lamb-Retherford apparatus.<sup>19</sup> In the earlier investigations on H,  $n = 2$ , a beam of metastable 2S atoms was made to travel a distance of about 10 cm to a tungsten plate from which an electron could be ejected by a collision of the second kind. A radio-frequency effect occurred when an appropriate microwave electric field connected a long-lived ( $\frac{1}{2}$  sec) 2S state to a short-lived ( $1.6 \times 10^{-9}$  sec) 2P state at some point along the beam. Variation of an external magnetic field in the rf interaction region produced a resonance at the detector that corresponded to changes in the numbers of 2S atoms reaching it as a function of the magnetic field. For  $n > 2$ , the  $nS$  states can radiatively decay to lower  $P$  states with the emission of a single photon ( $\Delta L = +1$ ), whereas the 2S state decays via two-photon emission and thus has a long lifetime. For thermal velocities (at room temperature) of  $1.4 \times 10^5 \text{ cm/sec}$ , a helium ion in the 4S state, which has a lifetime of  $1.4 \times 10^{-8}$  sec, will travel only about 0.02 mm before decaying. Hence, a beam experi-

ment is not possible. Instead, a method initially developed for He<sup>+</sup>,  $n = 2$  fine-structure investigations<sup>21</sup> and later used in other experiments on He<sup>+</sup>,  $n = 2$  as well as in ones examining the short-lived states of H,  $n = 3$ <sup>17,18</sup> is employed for the present He<sup>+</sup>,  $n = 4$  observations. Figure 5 shows an exploded view of the present electron gun region, while Fig. 6 presents a schematic diagram of the experimental arrangement. The equipment used in the measurements will be described in the following sections under the headings: electron gun, optical system and preamplifier, microwave system, magnetic field and its measurement, and finally, gas supply and pumps. Recently, parts of this same apparatus have been used to make studies of the  $n = 2$  fine structure in hydrogen.<sup>23</sup>

### B. Electron Gun

The electron gun shown in Fig. 5 is one part of a triode assembly which sends an electron beam across the waveguide structure parallel to the magnetic field. Not shown in this sketch is a grid placed between the emitting face of the cathode and the entrance perforations in the waveguide wall. Similar perforations exist on the opposite side of the waveguide through which the electron beam ultimately passes en route to collection by an anode plate which also is not shown. The grid and anode are grounded, whereas the cathode is at  $-400 \text{ V}$ .

Gun-current regulation was accomplished by the reaction of a feedback circuit upon the filament's heating current to any changes in the monitored excitation current. These filament-current corrections were necessary because of temporal changes in the detected current and because of magnetic field effects on the electron optics. The electron gun current regulator is depicted in Fig. 7. The regulator maintained the excitation current constant

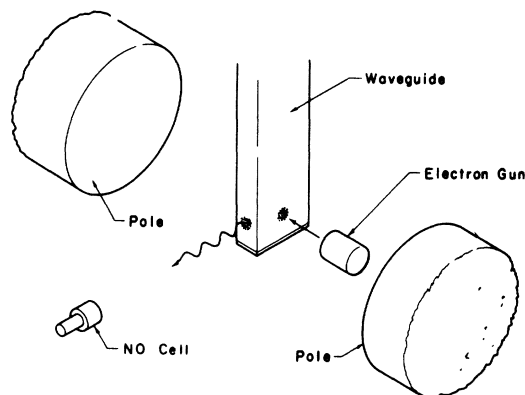


FIG. 5. Enlarged view of the electron bombarder region. The electron gun, waveguide, and magnetic field directions are oriented to study a  $\pi$ -type resonance (i. e., one in which  $\Delta m_L = 0$  for the transition involved).

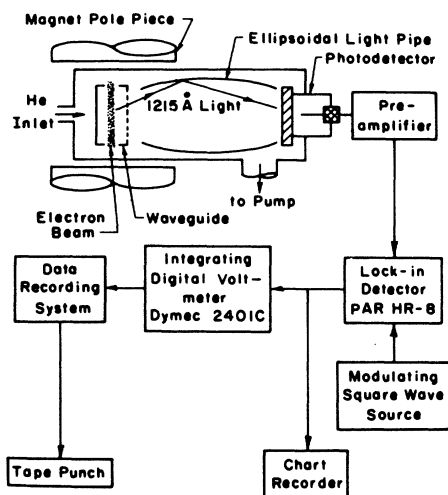


FIG. 6. Schematic diagram of the experimental apparatus. A resonance in the intensity of the 1215-Å light occurs when the external magnetic field is varied over suitable ranges for a fixed frequency of oscillating electric field in the waveguide.

to a few parts in a thousand over half-hour periods. Alternating current, rather than direct current, heated the bifilar wound tungsten filament to avoid the necessity of making possible corrections to the measured magnetic fields in the interaction region.

The Philips Metalonics cylindrical cathode, 0.95 cm in diameter and 1.4 cm long, consisted of a barium-activated tungsten surface ("type A") attached to the end of a molybdenum cylinder. Typical rms values for the filament current and voltage were 7 A and 6 V, respectively, when the emission current was several mA. Care was taken to use only nonmagnetic materials in the gun structure. Metallic gun materials were either molybdenum or tantalum, while the supporting struts and insulating spacers were constructed of alumina. Degreasing and outgassing of the gun parts was standard procedure before each data-taking period.

### C. Optical System and Preamplifier

The light from the interaction region passed through holes in the waveguide structure, as shown in Figs. 5 and 6, was collected by an ellipsoidal light pipe, and focused onto a nitric-oxide-filled gas cell having a magnesium fluoride ( $\text{MgF}_2$ ) window. The interaction volume within the waveguide and the uv detector were situated at the two foci of the ellipsoidal mirror. The NO cell and preamplifier are shown in Fig. 8. The output of the cell went to the input of an operational amplifier which was connected to either a lock-in detector or an integrating digital voltmeter, depending on whether the resonant signal, which was modulated at the lock-in reference frequency, or the total light sig-

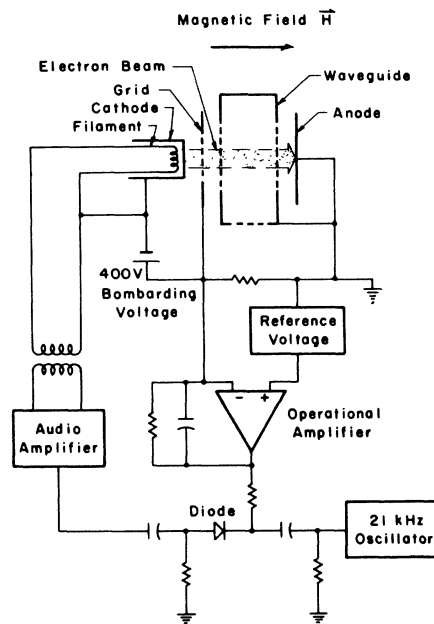


FIG. 7. Schematic diagram of the electron gun current regulator.

nal was to be monitored.

The NO gas cells were manufactured by Melpar Inc. and had quantum efficiencies at 1215 Å between 35% and 50%. They were 5.5 cm long; 3.3 cm in diameter and were filled to 20 Torr of NO. The 3.2-cm-diameter magnesium-fluoride window was sealed to the aluminum body of the cell with a cement of silver chloride. The wavelength passband of the cell was limited on the low side by the transmission

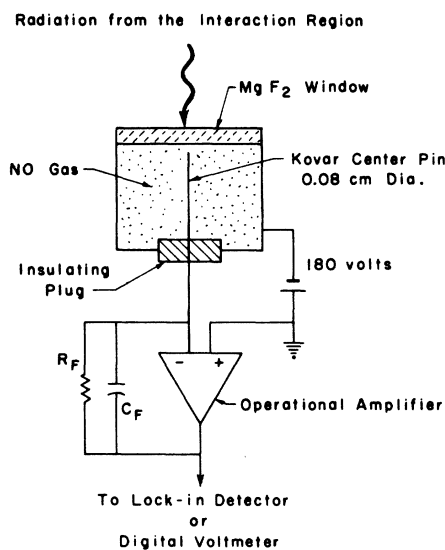


FIG. 8. Schematic view of the NO cell and the associated preamplifier.

cutoff of MgF<sub>2</sub> at about 1180 Å and on the high side by the first ionization threshold of NO at 1343 Å.

Two different operational amplifiers were used: the first, an Analog Devices No. 301 which was of the varactor-bridge variety; the second, a field-effect-transistor (FET)-type, Analog Devices No. 1401A. The former was used with a 10<sup>8</sup>-Ω feedback resistor ( $R_F$  in Fig. 8), while the latter version, using  $R_F$  equal to 10<sup>10</sup> Ω significantly improved the signal-to-noise ratio and thereby reduced the amount of data-taking time. Since both amplifiers were quite susceptible to microphonic noise pick-up, the inputs were buttressed directly against the NO cell's output pin. The NO cell and the attached preamplifier were housed together within a μ-metal magnetic shield 6.3 cm in diameter and 13.4 cm long. A strong portable magnet produced no discernible effect on the signals from the amplifier when it was held near this assembly. Thus, it was concluded that the fringing fields from the 12-in. Varian magnet at the uv detector, a distance of about 0.75 m, were incapable of producing a significant systematic error.

A highly polished ellipsoidal-mirror light pipe increased the light-collection efficiency of the detection system by a factor of 50 as compared with the case when no light pipe was used. The distance between foci is 71 cm, the minor axis is 9.7 cm long, and the entrance aperture is 3.3 cm wide. A section of the light pipe near the interaction region and within the magnet was made of oxygen-free high-conductivity copper (OFHC), while the remainder was made of stainless-steel alloy No. 316.

#### D. Microwave System

The transitions  $\alpha c$  and  $\beta d$  used to determine  $\Delta E_4 - s_4$  were studied at radio frequencies near 16 and 17 GHz ("P-band"), while the  $\alpha e$  and  $\beta e$  resonances, which yielded a value for  $s_4$ , required microwave frequencies between 8 and 9 GHz ("X-band"). Since these frequencies do not conveniently overlap within the same microwave equipment range, two different rf arrangements were used in the high- and low-frequency studies. They differed in some details but the essentials of the microwave system shown in Fig. 9 for the  $\Delta E_4 - s_4$  studies were duplicated for the  $s_4$  measurements.

The 16- and 17-GHz Varian reflex klystrons had tuning ranges of  $\pm 250$  MHz and typical peak output power of 1 to 1½ W, which in practice were diminished by use of a precision attenuator. Frequency locking of the klystron was established by means of a Dymec 2650-A oscillator synchronizer which supplied a correction to the klystron reflector voltage for any changes in the sampled frequency. The stability-determining factor was the synchronizer's crystal reference oscillator which was constant to a few parts in 10<sup>7</sup>.

The rf next passed through a low-pass filter and then through a ferrite isolator, which prevented reflected microwaves from interfering with the klystron's performance. The  $p-i-n$ -diode attenuator switch served the dual function of modulating and amplitude leveling the microwave radiation. A modulation frequency of about 40 Hz was employed. The crystal detector farther down the waveguide system sampled the rf power, and its output was compared with a reference voltage in the leveler modulator. Any necessary corrections were applied to the bias voltage of the  $p-i-n$  diode. The square-wave generator, in addition to supplying its output to the leveler modulator, also directed a part of this same signal to the lock-in reference frequency input. Thus, phase-sensitive detection of the 1215-Å light signals was achieved by 100% square-wave amplitude modulation of the microwave field. The "rf-off" half-cycle at the microwave switch had an associated 45-dB attenuation. Beyond the switch was a thermistor mount and power meter which detected a portion of the rf power reaching the interaction space. The microwaves eventually passed through a  $P$ - to  $X$ -band tapered section and a microwave pressure window to reach the interaction region defined within a section of  $X$ -band waveguide.

Frequency measurement was accomplished by use of the indicated circuit in Fig. 9 which was occasionally substituted for the crystal detector. In operation, a  $P$ -band mixer combined a harmonic of the transfer-oscillator fundamental frequency with the sampled klystron frequency such that the former was synchronized to produce a beat frequency of 30 MHz with the latter. Detection of the synchronization was achieved by use of the transfer-oscillator synchronizer while a frequency counter [Hewlett-Packard (HP) 5245L] measured the oscillator fundamental. The frequency-counter crystal reference was calibrated against an ultrastable quartz oscillator (HP 106B). The error in the frequency-measurement system is taken to be at most a few parts in 10<sup>7</sup>.

The modifications made to the rf line shown in Fig. 9 for the lower-frequency studies were slight and essentially involved substitution on a one-to-one basis of  $X$ -band for  $P$ -band devices. The low-frequency microwave source was a backward-wave oscillator sweep generator used in conjunction with a travelling-wave tube amplifier which together produced a net output power comparable to the 1 W of the klystrons.

#### E. Magnetic Field and Its Measurement

The  $X$ -band waveguide section containing the interaction region was positioned in the 3½-in. gap between the 12-in.-diam pole faces of the Varian (V-3603) regulated electromagnet. A Hall-effect probe affixed to one pole face monitored the mag-

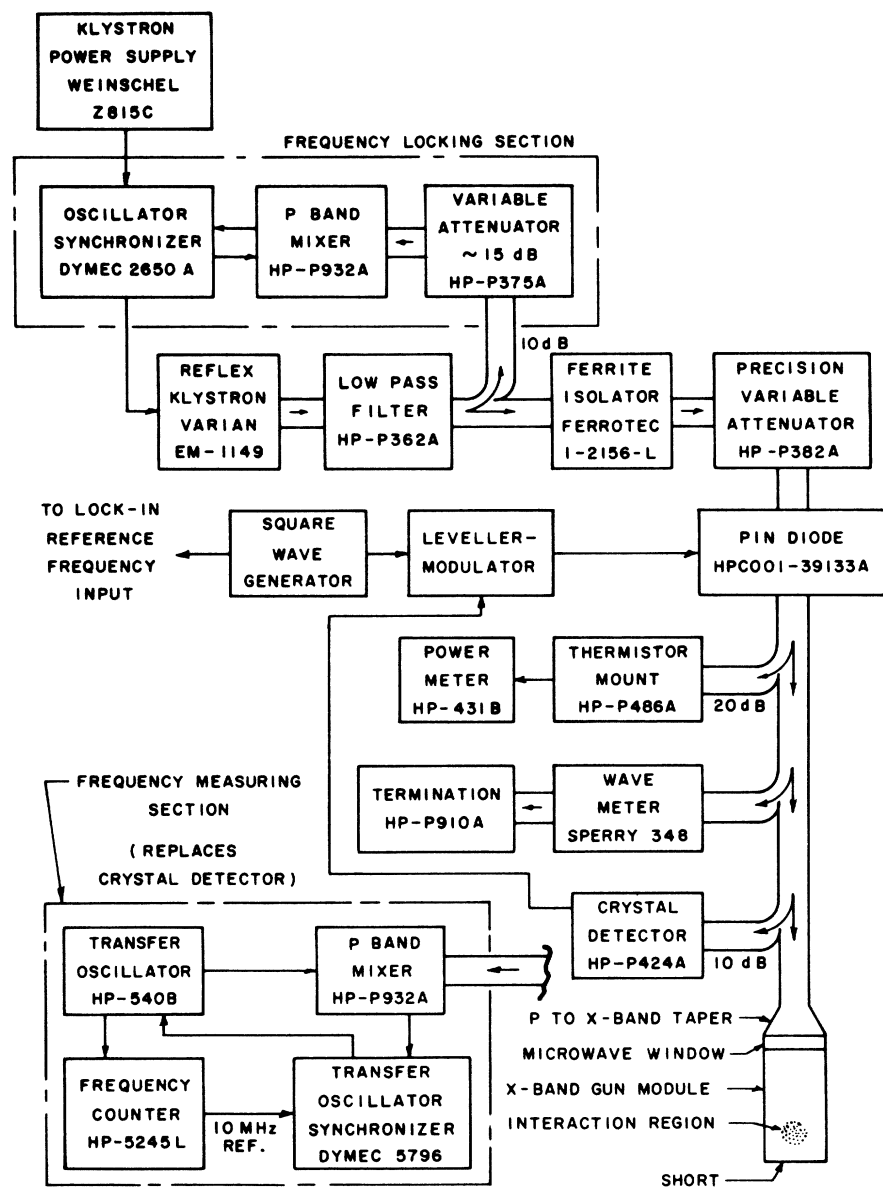


FIG. 9. Microwave system used in the  $\Delta E_4 - S_4$  studies.

netic field. For any field changes, the probe initiated a correction signal which was applied to the magnet from its power supply (V-FR-2503). Field drifts amounted to about 20 ppm per half-hour, but since most data runs took less than this time, such change was acceptable.

A nuclear-magnetic-resonance (NMR) system was used to measure the magnetic field. It consisted of a proton-resonance probe and a Magnion marginal oscillator (G-502). It is convenient to transform those terms in the Zeeman Hamiltonians that contain the magnetic field to circular frequency units in the following way:

$$g_S \mu_0 H / \hbar = f g_S / g_P', \quad g_L \mu_0 H / \hbar = (f g_S / g_P') g_L / g_S,$$

where  $g_S / g_P' = 658.22759$  is the ratio of the gyromagnetic ratio of the free electron to that of the proton in water<sup>24</sup> and  $f$  is the NMR circular frequency. The values for  $g_S$  and  $g_L$  are listed in Table I. The probe was secured in a slot attached to the experimental housing near the center of one pole face and outside the vacuum system. Since the magnetic field is not measured at the site of the interaction region, the vacuum system was periodically opened to permit the repositioning of the probe in the volume occupied by the waveguide gun module. The results of measuring the magnetic field in the experimental region and in the slot, a separation of 3 to 5 cm, were such that corrections had to be applied to most of the data. The magnetic

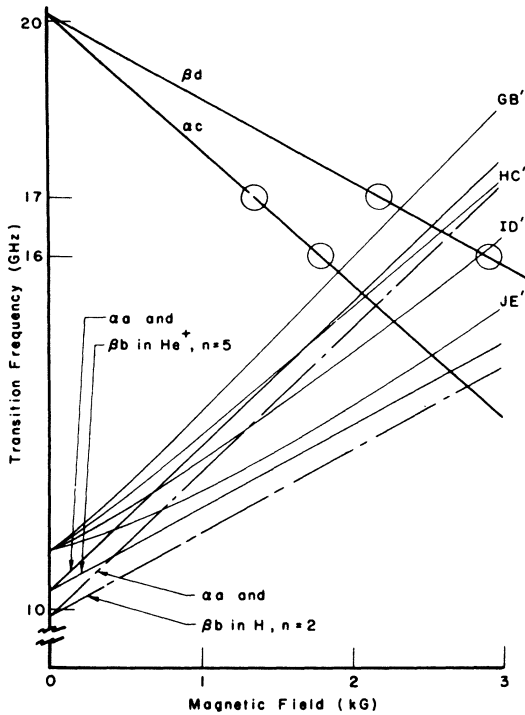


FIG. 10. Various electric dipole transition frequencies versus magnetic field near the  $\Delta E_4 - S_4$  data-taking regions.  $|\Delta J| = 2$  transitions are denoted by capital Roman letters and follow the notation of Fig. 2. The circles mark the areas investigated.

inhomogeneity over the interaction region was measured by a proton-resonance probe to be 17 ppm along the field axis (the "z direction" in the experiment) and 10 ppm in the radial direction. These inhomogeneities have a negligible effect on the results.

#### F. Gas Supply and Pumps

Helium with a specified hydrogen impurity of less than 1 ppm was obtained from the Matheson Co. The gas passed from the tank through a regulating valve with a two-stage metal diaphragm and entered the vacuum system through a length of stainless-steel capillary tubing. In order to reduce the effects of temperature changes on the input-leak rate, this tubing was immersed in an oil bath. The pressures used in the experiment varied from  $0.5 \times 10^{-3}$  to  $40 \times 10^{-3}$  Torr and were continuously monitored by a Pirani gauge (Consolidated Vacuum Corp. GP-210) calibrated for air.

The pumping station consisted of a Welch 3102-A turbomolecular pump followed by a Welch two-stage mechanical forepump. A nearly vibration-free condition of the experimental housing was achieved by means of two sections of stainless-steel bellows which connected the pump to the vacuum envelope of the apparatus. The ultimate vacuum achieved

by the pump with no helium passing through the system was  $6 \times 10^{-7}$  Torr as determined by a Heraeus Ionivac 2 ionization gauge. A partial-pressure gauge (Varian 974-0035) indicated that this residual background was primarily air and water vapor.

### III. MEASUREMENTS

#### A. Choice of Transitions and General Investigations

Here we present a few of the problems involved in selecting particular transitions for study as well as the results of certain general investigations on these transitions.

A major point to stress in considering fine-structure studies in hydrogenic systems utilizing the present technique is that certain transitions are strongly affected by overlapping resonances, both from the term under study and by cascade from higher-lying  $n$  states. To illustrate the point, one need only compare the plots of transition frequency versus magnetic field given in Figs. 10 and 11. The first graph shows the location of the  $\alpha c$  and  $\beta d$  working points used in the determination of  $\Delta E_4 - S_4$ . The second graph shows the numerous  $n=4$  overlapping transitions involved in the study of the Lamb shift  $S_4$  using the  $\alpha e$  and  $\beta e$  transitions, as well as those resonances due to cascades from  $S-P$  transitions in  $n=5$ , denoted (5), and finally those transitions in hydrogen,  $n=2$ , denoted (H), which can add to the signal. The inclusion of cascade effects from higher  $n$  states in the fitting function assumes that any microwave transitions between their sublevels contribute to the observed signal in an additive manner such that the signal shape is a sum of expressions like that given in Eq. (3). That is, any rf transition in these higher  $n$  states can be observed as a change in the 1215-Å light intensity as these levels decay through the  $n=4$  level en route to the ground state of the ion. Also, contributions from other dipole resonances in  $n=4$ , including those generated by an rf electric field of the undesired polarization, are assumed to contribute in this additive fashion. For these reasons, the  $\alpha c$  and  $\beta d$  transitions were the first ones studied instead of the potentially more complicated  $\alpha e$  and  $\beta e$  resonances which were examined later. The  $|\Delta J| = 2$  transitions shown in Fig. 10 have an entirely negligible effect on the  $\alpha c$  and  $\beta d$  results, as do the transitions in  $\text{He}^+$ ,  $n=5$  and  $\text{H}$ ,  $n=2$ . Figure 12 shows a scan of the  $\alpha c$  and  $\beta d$  resonances taken under typical experimental conditions. In it, the  $\alpha c$  resonance is rf power broadened from a natural width of 100 to about 150 G while the  $\beta d$  resonance is broadened from 150 to about 300 G. Since the fine-structure separation varies approximately as  $1/n^3$ , rf transitions between Zeeman sublevels in states for  $n \geq 5$  can have but a slight resonant cascade effect on the  $n=4$  transitions that determine

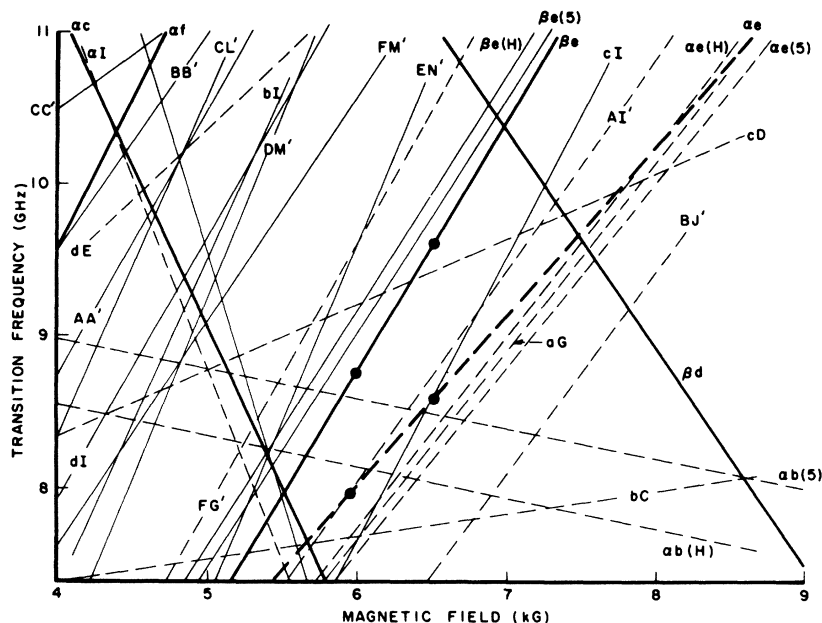


FIG. 11. Various electric dipole transition frequencies versus magnetic field near the  $S_4$  data-taking regions. The dots represent the specific areas studied. Solid lines represent  $\sigma$ -type transitions, and dashed lines represent  $\pi$ -type transitions.

$\Delta E_4 - S_4$ , because the transition frequencies in the  $n \geq 5$  states are much smaller than those used for the  $ac$  and  $\beta d$  working points. This fortunate situation does not exist for the  $S_4$ -determining resonances, since they can be affected by transitions in these higher- $n$  states as well as by the numerous nearby  $P$ - $D$  and  $D$ - $F$  resonances in  $n=4$ . Figure 11 contains the  $ae$  and  $\beta e$  data-taking points and is favorable over other  $S_4$ -providing transition regions, which have many more interfering resonances. Figure 4 showed only  $S$ - $P$  transitions in  $n=4$  since the inclusion of all possible electric-dipole transitions, which would involve the  $D$  and  $F$  levels as

well, would make too complicated a diagram. As seen by referring to the basic line-shape expression given in Eq. (3) and the subsequent discussion, any undesired interlopers could be exactly accounted for if the excitation rates (i. e.,  $r_L$ 's) were known. Unfortunately, they can be theoretically determined only to an order of magnitude,<sup>21,25</sup> while experimental information on them is almost negligible.<sup>26</sup> Because of these uncertainties, the  $S_4$  measurements are more limited in accuracy than the  $\Delta E_4 - S_4$  measurements. Figure 13 shows a scan of the  $\beta e$  resonance under typical experimental conditions. Chart tracings of a number of other  $S_4$ -determining

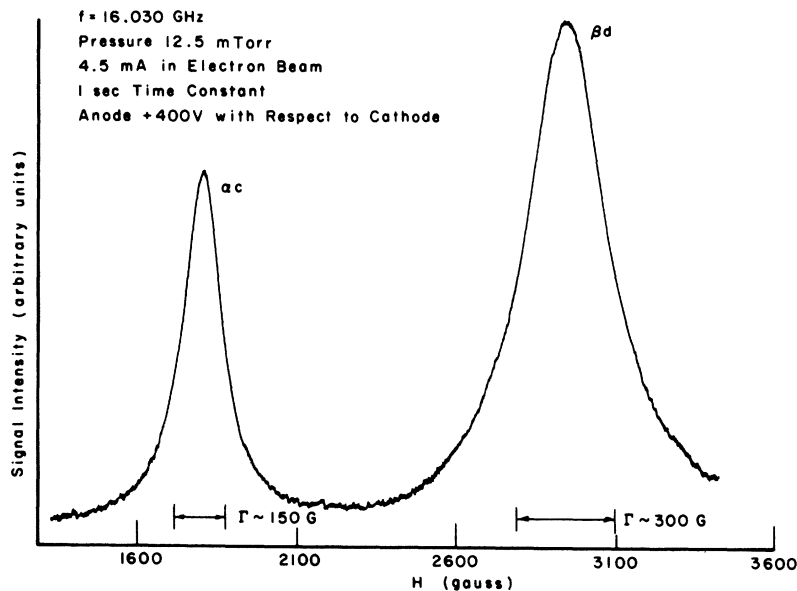


FIG. 12. Recorder tracing of the  $ac$  and  $\beta d$  resonances in the  $n=4$  term of singly ionized helium. These transitions yield values for  $\Delta E_4 - S_4$ . This trace took about 10 min to produce.

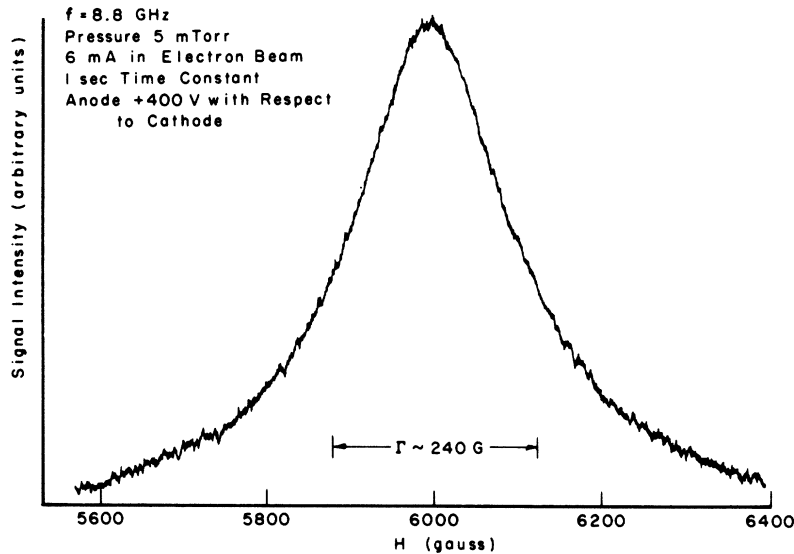


FIG. 13. Recorder trace of the  $\beta_e$  resonance. This transition gives a value for  $S_4$ .

resonances were quite visibly skewed because of overlapping signals. Since the natural linewidth of the  $n=4$   $S$ - $P$  resonances is about 218 MHz (due primarily to the short-lived  $P$  state), accuracies comparable to earlier fine-structure measurements would require locating the resonance centers to  $\pm 0.2$  MHz or to one part in a thousand of the natural linewidth.<sup>19</sup> As will be seen later, this was not possible in the present work because of incompletely understood systematic effects.

The remainder of this section will illustrate the following four experimental investigations: (a) observation of an  $S$ - $D$  resonance, (b) a  $\beta$ -state quenching phenomenon near 2000 G due to  $z$ -type electric fields which couple the  $\beta$  and  $f$  states at the  $\beta f$  crossing, (c) a typical excitation curve, and (d) a typical microwave-power saturation curve.

In the course of study on the  $\beta_e$  resonance, it was observed that the  $\alpha c$  transition, which was usually located far into the tail of  $\beta_e$ , had some structure superimposed on it. This fact is demonstrated by the "notch" in  $\alpha c$  as shown in the upper half of Fig. 14. The bottom half shows the effect on the three resonances of changing to a lower microwave frequency; in particular, it is seen that the notch can be positioned at the peak of the  $\alpha c$  resonance. The occurrence of this notch can be explained with the aid of the energy level diagram in Fig. 15. In it we see that a static  $x$ -directed electric field can couple the  $c$  and  $E$  states. The magnitude of the coupling will exhibit a resonance effect as the magnetic field passes through the region where the levels cross. This phenomenon can be described by Eq. (3) with the changes  $\nu = 0$  and  $|V|^2 = 4|V|^2$ . Thus, a two-stage process, namely, the rf coupling between  $\alpha$  and  $c$ , along with the electrostatic coupling between  $c$  and  $E$  makes possible an  $\alpha$  to  $E$  tran-

sition. The theory for this dual-coupling situation would require slight modifications to the three-level problem developed in Ref. 18. Precision studies of this  $S$ -to- $D$  transition were not attempted, but the signal strengths observed along with the reduced linewidth relative to the  $S$ - $P$  transitions (82 MHz versus 218 MHz) suggest the possibility

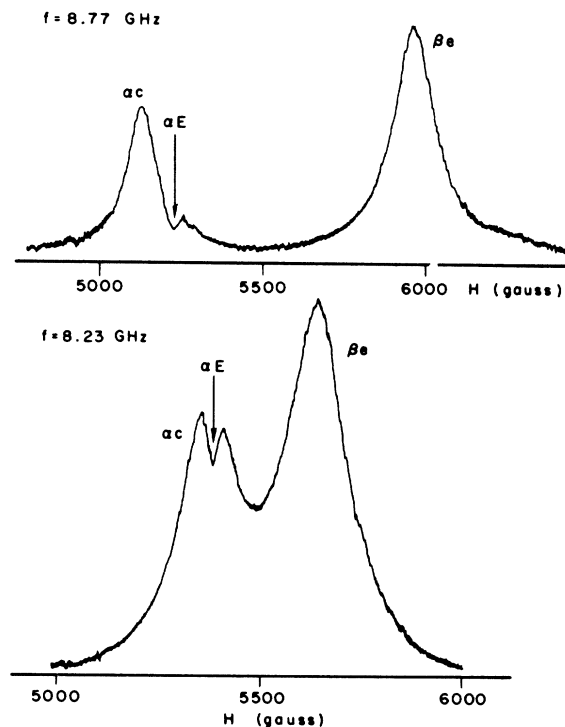


FIG. 14. Recorder trace of the  $S$ - $D$  resonance  $\alpha E$  showing its position relative to  $\alpha c$  and  $\beta_e$  for two microwave frequencies.

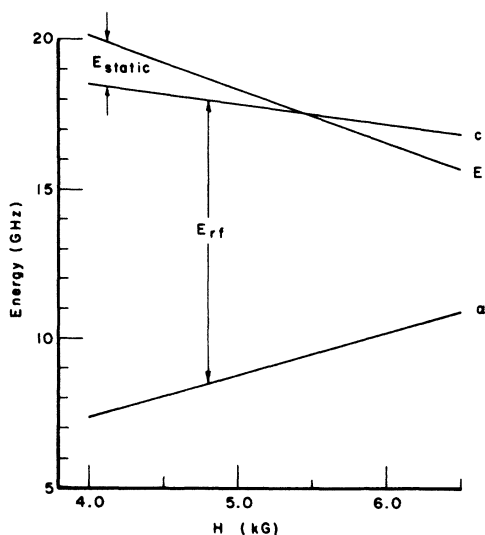


FIG. 15. Energy levels involved in observing the  $S$ - $D$  transition  $\alpha E$ . The rf coupling between  $\alpha$  and  $c$  and the static coupling between  $c$  and  $E$  are indicated. The amplitude of the  $S$ - $D$  resonance exhibits a maximum at the magnetic field where  $c$  and  $E$  cross.

of making a precision measurement to determine the quantity  $\Delta E - s - \Sigma + \Delta E$  shown in Fig. 2.

More quantitative studies were made on a similar three-level situation which involved the  $\beta d$  transition and the  $f$  state. From the transition-frequency diagram of Fig. 4, we see that for a microwave frequency near 17.4 GHz, studies on  $\beta d$  would be affected by the coupling of states  $\beta$  and  $f$  via  $z$ -directed electric fields near the  $\beta f$  crossing. Figure 16 illustrates the quenching of the  $\beta d$ -resonance amplitude relative to that of  $\alpha c$  due to an increase in the electron-excitation current. Such a marked reduction in the  $\beta d$ -to- $\alpha c$  height ratio did not occur at the 16-GHz operating point. Further discussion is given in Sec. IV B dealing with the effect of the  $\beta f$  crossing on the  $\beta d$  resonance.

A third investigation is shown in Fig. 17, which depicts a typical excitation curve. This result is representative of the  $\alpha c$ ,  $\beta d$ , and  $\alpha e$  cases as well as the cited  $\beta e$  one. Three features are to be noted from this figure: First, the theoretical threshold voltage of 75.6 V for the helium ion,  $n=4$  excitation is fairly well confirmed in the signal curve; second, the excitation rises quite rapidly up to about 200 V and then begins approaching a fairly constant value at the working voltage of 400 V; and third, the "foot" in total light intensity below the  $n=4$  threshold, which is discussed in Sec. III B.

The fourth study is shown in Fig. 18, in which we present a representative study of the lock-in signal at a  $\Delta E_4 - S_4$ -determining resonance center as a function of the rf power. The computer-fitted curve for the depicted  $\beta d$  signal used the indicated simple

fitting function which is just Eq. (3) with  $\omega = \nu$ .

#### B. Normalization of Signal

Normalization of the 1215-Å light signal is desirable for at least two reasons. First, since the electron gun and interaction region are located in a magnetic field, the effective rates for the ionization-excitation process, which transfers some helium atoms to the  $n=4$  state of the helium ion, may be magnetic field dependent. One such field-related effect is the variation in excitation current due to the electron beam's interception by the honeycomb structure in the waveguide wall. Second, since the signals in the experiment were integrated for lengthy time periods, i. e., 100 sec, drifts in the conditions existing in the interaction region, e. g., pressure, were possible. To overcome these adverse effects on the data, two different normaliza-

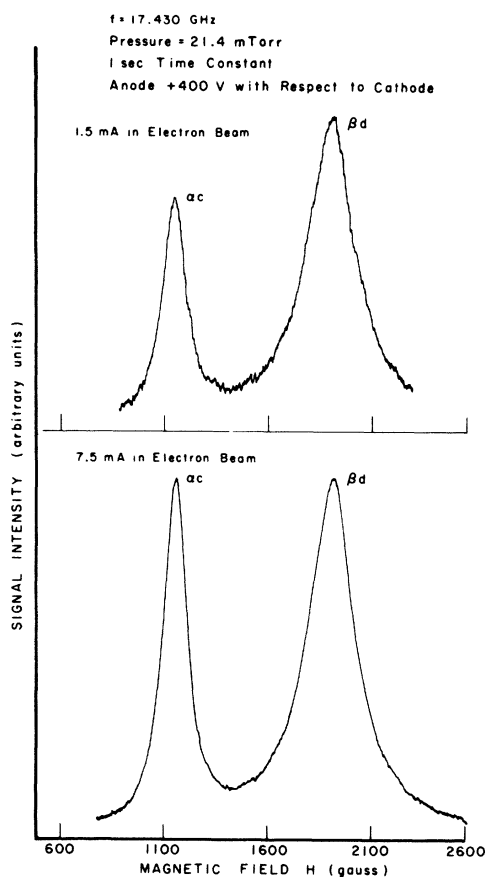


FIG. 16. Depicted in the chart tracings is a reduction of the  $\beta d$ -to- $\alpha c$  amplitude ratio for an increase in the exciting electron current. A corresponding increase in the magnitude of the  $z$ -directed electric field due to such a current change would increase the coupling between the  $\beta$  and  $f$  states at the  $\beta f$  crossing and hence cause a reduction in the  $\beta d$  amplitude. It is noted that the two signal scales have different ranges.

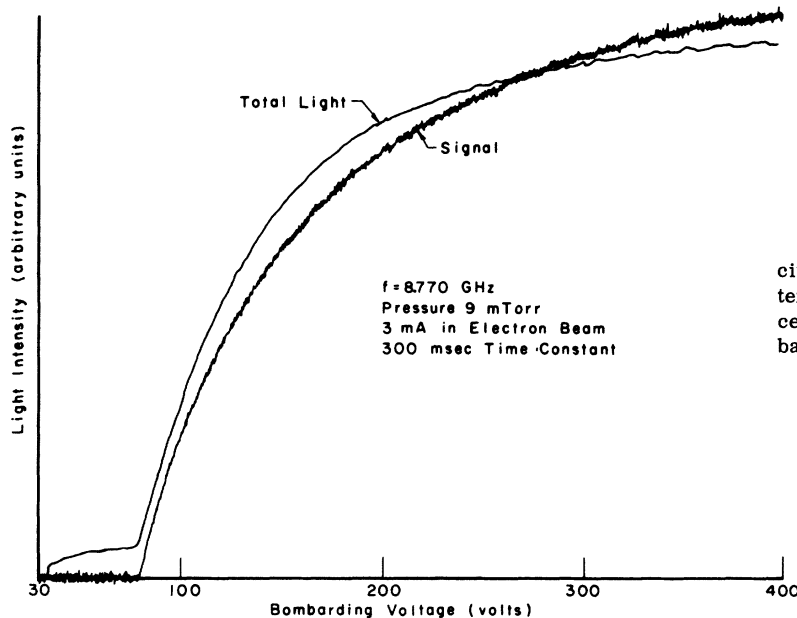


FIG. 17. Reproduction of a typical excitation curve showing the total light intensity and the rf signal at the  $\beta e$  resonance center as a function of the electron-bombardment voltage.

tion schemes were used. One method depended on dividing the resonance signal by the total light intensity measured by the NO cell, while the other involved dividing the resonance signal by a second resonance signal taken at a considerably higher rf power level than the first.

Unfortunately, each of these normalization procedures had its own difficulties. Since the normalizing quantity is intended to be proportional to the total number of available helium ions in a particular 4S sublevel, one must ensure that light from other sources is not introducing any appreciable error. For example, water vapor could be decomposed by the electron bombardment and produce Lyman- $\alpha$  (1216 Å) radiation which would then contribute to the total light intensity. The excitation curve of Fig. 17 indicates a total light signal below the theoretical threshold of 75.6 V for the excitation of helium ion,  $n=4$ . This intensity was due in part to Lyman  $\alpha$  and in part to light of unknown origin, possibly from the helium atom.<sup>27</sup> An upper limit for the NO cell's detected radiation (1180 - 1343 Å), not attributable to Balmer  $\beta$  from the helium ion, was about 10 to 15% of the total light signal. Such light, unaccounted for, would not introduce error in the normalization if one were operating at a frequency which did not produce a resonance between the involved levels, or if there were no differential angular distribution between it and the desired radiation, i. e., if this light intensity were not magnetic field dependent.

The "rf normalization" scheme concentrates on a particular helium-ion transition by using two modulated signals of considerably different intensity. This second procedure produces a normalizing signal

that is also proportional to the total number of helium ions in one of the 4S substates. Now, however, a cataloging of various 1215-Å light sources is not necessary since the normalizing signal is modulated. Again, this assumes one is not observing resonances due to unknown ultraviolet sources. Unfortunately, since this rf normalization technique divides one lock-in signal by another, the resultant data have more noise in them than when the normalizing quantity is the more stable total light intensity.

#### C. Procedures in Data Taking and Analysis

For reasons given in Sec. III A, precision measurements were made on the four transitions indicated in Fig. 3. Two different data-taking procedures were used. One technique involved selecting

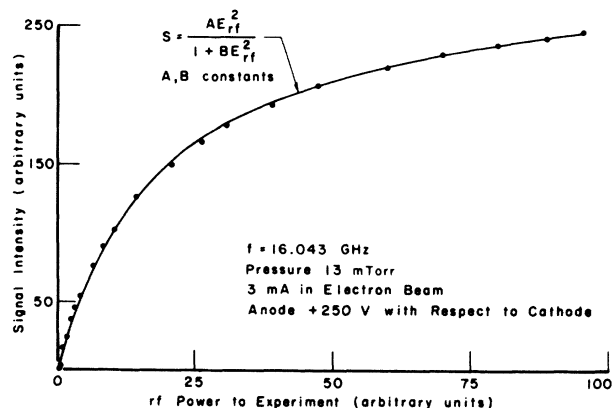


FIG. 18. Computer fit to the experimentally measured amplitude of the  $\beta d$  resonance center as a function of the rf power.

three magnetic field values that corresponded to the center of the resonance under study and two points on either side of the center where the signal had decreased to between one-half and three-quarters of the maximum intensity. In the second method, 15–20 magnetic fields were chosen, so that the resultant plot of the signal intensities gave a panoramic view. The first procedure allowed one to test the dependence of the fitted values for  $\Delta E_4 - S_4$  or  $S_4$  on the various experimental conditions in a relatively short time. The second procedure of panoramic data taking allowed one to test more sensitively various line shapes on a complete resonance before applying them to the three-point investigations. The multipoint panoramics were quite time consuming since the data at a given magnetic field took about 5 min to accumulate. Thus, the over-all stability of the system had to be excellent, even though the normalization compensated for small drifts in the experiment during the time required to complete data taking at one magnetic field.

For a selected magnetic field, six items of data were recorded: (a) the NMR frequency, (b) the lock-in signal at a low rf power level, (c) the lock-in signal at a high rf power level, (d) the lock-in zero, i.e., the signal with the rf off, (e) the total light signal from the NO cell with the rf off, and (f) the zero for the total light signal which in practice required a shorting to ground of the input of the operational amplifier shown in Fig. 8. The signals from the lock-in detector were integrated for 100 sec, whereas the photocell's current due to the total light intensity was integrated for 10 sec. Once a particular magnetic field value was obtained, a scanning cycle was begun which punched the values that corresponded to the previously itemized quantities on paper tape after they were measured by an integrating digital voltmeter or, in the case of the NMR signal, by a frequency counter. At the completion of such a scan, the magnet's power supply automatically changed the magnetic field to the next value. The NMR oscillator was then set manually to the proton resonance frequency of the new field point and another data-recording cycle was initiated.

Other pertinent quantities that were manually recorded for the various runs included the pressure, the microwave frequency, which was periodically measured and found to be reproducible and stable to at least one part in  $10^7$ , the electron gun current, the bombarding voltage, and the microwave power levels directed toward the interaction region.

The punched paper tape was then processed by an IBM 46 tape-to-card converter. The resultant data cards were handled by a computer program that diagonalized the Hamiltonian as discussed in Sec. IC. The fitting function for the data contained at least three parameters. For the total light normalization scheme, they were the amplitude and center

of the resonance as well as the rf electric field strength. For the normalization procedure using the low-rf signal divided by the high-rf signal, the three basic parameters were the two rf electric field magnitudes and the resonance center. Additional parameters corresponded to quantities introduced into the line shape to take into account the many possible corrections to be discussed in Sec. IV.

Figure 19 depicts the result of a typical fit to resonance data. The line-shape function which was used consisted of two expressions like that of Eq. (3) – one for the main  $\beta d$  resonance and one for overlap from  $\alpha c$ .

#### IV. SOURCES OF ERROR AND THEIR CORRECTIONS

##### A. Stark Shifts and Quenching

Static electric fields in the experimental interaction region will cause Stark shifts of the energy levels in the excited helium ions. Four sources of such fields are (a) electron gun accelerating electric fields which may penetrate through grids into the waveguide, (b) unneutralized space charge in the electron beam, (c) charges accumulated on layers of insulating material deposited on or near the waveguide structure, and (d) the motion of an ion through the magnetic field which gives a motional field  $\vec{E} = (\vec{v}/c) \times \vec{H}$ . From the schematic diagram given in Fig. 7 it is seen that the electrodes surrounding the waveguide structure were all kept at ground potential. This was done to prevent any fields from penetrating into the interaction region.

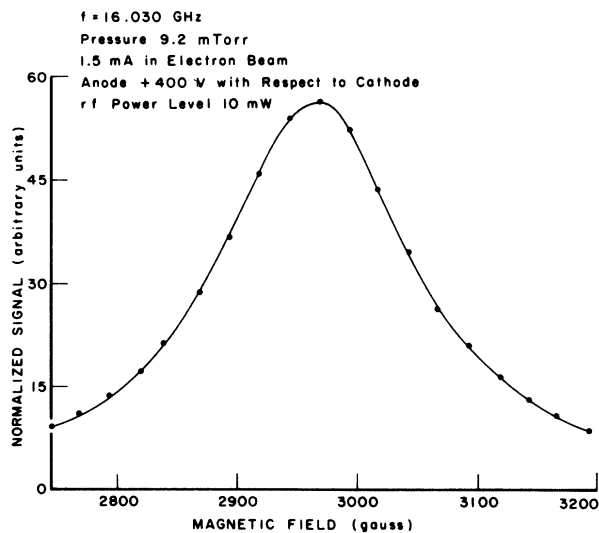


FIG. 19. Computer fit to the multipoint data of a  $\beta d$  resonance. Normalizing quantity is the total light intensity. Value for  $\Delta E_4 - S_4$  obtained from this analysis is  $\Delta E_4 - S_4 = (20180.25 \pm 0.30)$  MHz. The difference between the experimental and fitted quantities is less than the indicated dot size.

A generous upper limit of 2 V/cm is ascribed to the electric field due to leakage through the grids and to charged insulating layers. This value was determined from offsets in the threshold voltage for excitation to the  $n=4$  states which were observed under certain conditions, and by use of the three-level theory, which used such a static field as a parameter in analysis of data taken near the  $\beta f$  crossing. Assuming that the positive ions do not neutralize the electron beam, one can calculate the rms radial electric field due to a 1.50-mA beam emitted from a circular cathode surface 0.50 cm in diam, in which the electrons have an energy of 400 eV to be 6.4 V/cm. Of course, any helium ions formed in the beam will neutralize the electron space charge somewhat. It is felt that the other extreme alternative of a positive ionic space charge is not possible because of the many slow secondary electrons generated near the interaction region.

For  $T = 300^\circ\text{K}$ , the thermal velocity of a helium ion is  $|\bar{v}| = 1.39 \times 10^5$  cm/sec. The magnitude of the resultant motional electric field for  $\bar{v}$  perpendicular to the magnetic field  $\vec{H}$  is  $1.37 \times 10^{-3} H$  V/cm, where  $H$  is in gauss. For  $H = 2500$  G, the motional field is 3.42 V/cm; for  $H = 6500$  G, it is 8.90 V/cm. Figures 20 and 21 illustrate the Stark effect for the four transitions studied. These graphs were constructed by the computer diagonalization procedure described in Sec. I C. The Hamiltonian matrix was diagonalized first with the appropriate Stark elements included and then with them omitted. Figures 20 and 21 represent the differences between corresponding pairs of the four transition frequencies of interest for the two field directions. To obtain the magnitude of a frequency shift for another perturbing electric field, one may scale these results with the square of the field ratio. Finally, it can be shown that under the conditions of the present ex-

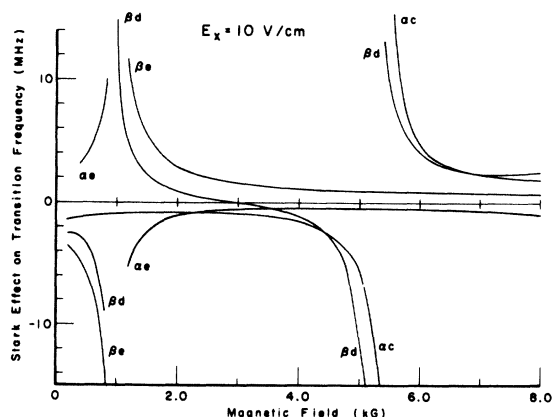


FIG. 20. Stark-effect shifts of the four transition frequencies used in the precision measurements assuming an electric field of 10 V/cm perpendicular to the applied magnetic field.

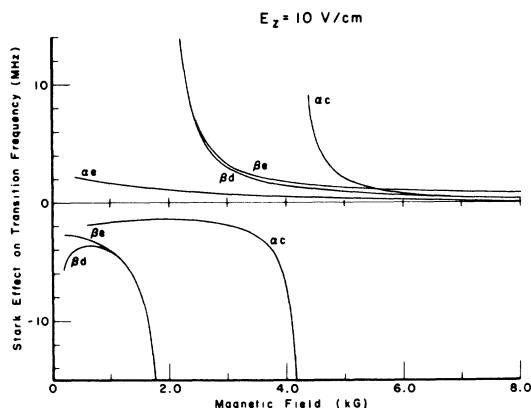


FIG. 21. Stark-effect shifts of the four transition frequencies used in the precision measurements assuming an electric field of 10 V/cm parallel to the applied magnetic field.

periment, magnetic-field-dependent quenching of the excited ions by static electric fields is significantly less important in affecting the resonance centers than Stark shifting of the energy levels.

#### B. Collisional Quenching

We now consider the effect of quenching the excited  $n=4$  states by the time-varying electric fields due to collisions with ions, atoms, and electrons. These transient fields have a greater effect through quenching than through shifting the energy levels, since the excited state lifetimes are much greater than the interaction times involved.

In attempting a description of the effect of collisions on the observed transitions, we were guided by a similar analysis which has been reported for the quenching of metastable hydrogen atoms in the solar chromosphere.<sup>28</sup> This latter derivation required proton velocities determined by temperatures of the order of  $10^4$  °K, so its results for ion quenching are not applicable to the present experiment. The treatment of electron quenching, however, is applicable for the present experimental conditions, but can be shown to be significantly less important than ion and atom quenching, and will not be considered further.

An excited helium ion, then, is subject to electric fields due to (i) other ions, and (ii) ion-induced dipole moments of helium atoms. These electric fields cause transitions between the excited states of the ion, contributing a term to the decay rates of the levels involved. The extent of this quenching depends not only on the strength and time variation of the perturbing electric field, but also on the energy separation of the coupled states. It will therefore vary with magnetic field. In addition, the quenching rates will depend on the excitation current  $I$  and the helium gas pressure  $P$ . Thus, quenching

by ions will vary with the ion population, which will depend on the product  $IP$ . Quenching by atoms will vary simply with  $P$ . The effective decay rate of the  $\beta$  state, for example, may be written

$$\gamma = \gamma_s + B_1 IP + B_2 P,$$

where  $B_1$  and  $B_2$  are magnetic-field-dependent proportionality constants. The  $\beta$ -state quenching mechanism is taken to be the  $\beta f$  crossing at 2000 G which would affect  $\beta d$ -resonance data. Ideally, one would use  $\gamma$ , rather than  $\gamma_s$ , in the expression for the resonance line shape when analyzing the data. However, this presupposes a quantitative knowledge of the coefficients  $B_1$  and  $B_2$ . Expressions for  $B_1$  and  $B_2$  were obtained by extending the development of Appendix II in H1<sup>19</sup> to the case where the perturbation  $V$ , connecting a  $4S_{1/2}$  state to either a  $4P_{3/2}$  or  $4P_{1/2}$  level, assumed a slow time dependence rather than just a static value. Numerical values for  $B_1$  and  $B_2$ , subject to the limitations of this quenching theory, were compared with values derived from least-squares fitting of experimental data. They were found to be too small by roughly a factor of 5. In view of this disagreement, it was decided that a more empirical approach should be adopted to take account of a possible shift of resonance center resulting from these quenching mechanisms. Line-center data (derived using natural decay times) were examined for dependence on  $IP$  and  $P$ . The four resonances studied in the present work were all found to exhibit some dependence on these parameters. By making a linear extrapolation to zero  $IP$  and  $P$ , it is expected that the line centers can be corrected for collisional quenching effects. This is further discussed in Sec. VB.

### C. Overlapping Resonances

As seen in Figs. 10 and 11 the  $\Delta E_4 - S_4$ -determining transitions  $\alpha c$  and  $\beta d$  suffered from far fewer potentially overlapping resonances than the  $S_4$ -yielding resonances  $\alpha e$  and  $\beta e$ . In fact, the only possible overlaps in the high-frequency studies were due to the  $\alpha a$  and  $\beta b$  transitions in  $\text{He}^+$ ,  $n=5$ , which become important via cascade of the  $n=5$  levels to the  $n=4$  states; the  $|\Delta J|=2$  transitions in  $\text{He}^+$ ,  $n=4$  shown in Fig. 10; and the  $\alpha a$  and  $\beta b$  transitions in the  $n=2$  level of hydrogen. The  $|\Delta J|=2$  resonances can occur because at finite magnetic fields the eigenstates become linear superpositions of the zero-field eigenstates of  $J$ . Fortunately, the small matrix elements of these transitions along with certain assumed excitation rates given in Sec. ID make these signals totally indistinguishable from the noise in the data. Also buried in the noise are the effects of overlap from  $\alpha a$  and  $\beta b$  in H,  $n=2$  as well as  $\alpha a$  and  $\beta b$  in  $\text{He}^+$ ,  $n=5$  at the fields where the  $\alpha c$  and  $\beta d$  precision investigations were made.

Unfortunately, the effects of the overlapping res-

onances in the  $S_4$  studies shown in Fig. 11 could not be dismissed as easily. The  $\alpha e$  and  $\beta e$  resonance centers exhibited a several megahertz shift when very low rf power levels were employed in the data taking. This striking dependence of the  $S_4$  transitions on the microwave power is depicted in Fig. 22, in which are plotted the resonance line centers for data normalized by the total light intensity. An analogous effect on  $\alpha c$  or  $\beta d$  was extensively searched for but was not observed. In an attempt to establish the cause of the rf power shift on the  $S_4$  data, the various transitions shown in Fig. 11 were systematically included in the line-shape expression used to computer analyze the  $\alpha e$  and  $\beta e$  multipoint panoramics. The importance of each effect was determined by its influence on the least-squares sum, i. e., the sum of squares of differences between the experimental and final fitted signal values across the resonance curve. First, the computer program adjusted the values of three parameters in the fitting function to produce the best fit for  $\alpha e$  data normalized by the total light intensity. The parameters were (i) an over-all multiplicative amplitude, (ii) the rf power level, i. e.,  $E^2$ , and (iii)  $\omega$ , the resonance frequency. Next, the following contributions to the normalized  $\alpha e$  signals were considered in the fitting function: (a) overlap from other nearby  $S$ - $P$  resonances in  $\text{He}^+$ ,  $n=4$  which depend on a polarization of the rf electric field orthogonal ( $\sigma$  type) to that necessary to observe an  $\alpha e$  resonance ( $\pi$  type); (b) overlap from nearby  $\pi$ -type  $P$ - $D$  resonances in  $\text{He}^+$ ,  $n=4$ ; (c) overlaps caused by  $S$ - $P$   $\pi$ -type resonances in  $\text{He}^+$ ,  $n=5$  which make their presence felt via cascades to the  $n=4$

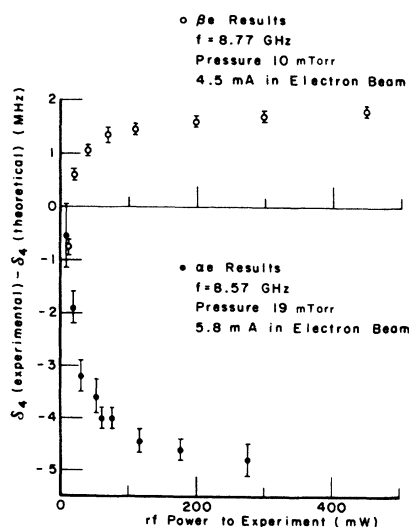


FIG. 22. Depicted are typical discrepancies between experiment and theory for the level shift  $S_4$  as a function of rf power to the experimental interaction region using data normalized by the total light intensity.

levels, thereby altering the rate Eqs. (1); (d) overlap from nearby  $\pi$ -type  $D$ - $F$  transitions in He<sup>+</sup>,  $n = 4$ ; (e) overlap from nearby  $\pi$ -type resonances in H,  $n = 2$ ; and (f) finally, the effect of rf transitions from the  $4P$  to the  $4D$  states and the subsequent effect on  $\dot{n}_p$  in Eqs. (1). None of these causes, when added individually to the Lorentzian line shape given in Eq. (3), was able to significantly reduce the least-squares sum below the one obtained with a line shape described entirely by Eq. (3).

A possible explanation of this rf power effect on the  $S_4$  data consistent with all the experimental evidence was a cascade effect due to the very many dipole transitions possible in the higher-lying  $n$  states. Transitions induced by the microwaves between suitable pairs of sublevels in these higher- $n$  states can cause magnetic-field-dependent changes in the populations of the  $n = 4$  levels, thus altering the rate Eqs. (1). The exact solution of the problem is a major undertaking, and even then, uncertainties in the values of the cross sections for electron excitation to these higher- $n$  states would put the results of such an analysis in question. A very rough approximation to such an exact treatment predicts that the net effect of transitions in these higher- $n$  states could shift the fitted resonance center in a  $1/E$  fashion for low rf power levels. Such a dependence on the microwave field strength is suggested by part of Fig. 22. Unfortunately, this prediction is based on a crude model and cannot be taken very seriously without further detailed computations made on a more refined model.

#### D. NMR Correction

As indicated in Sec. IIE, it was necessary to make corrections to the measured magnetic fields since the NMR probe was located in a slot a short distance away from the experimental interaction region. This correction had a larger effect on the  $S_4$  transitions, which were measured at higher magnetic fields, than on the  $\Delta E_4 - S_4$  transitions.

The magnetic field was measured at the site of the interaction region upon conclusion of a data-taking period – typically five weeks. Then, the gun module was removed from the vacuum chamber and a copper support, which held the NMR probe, was secured in its place. The probe was then alternated between the slot and interaction volume to determine any field difference. This difference was then converted to a correction in the value of either  $\Delta E_4 - S_4$  or  $S_4$  by use of an effective  $g$  value, at the working magnetic fields, for the particular transition being investigated.

#### E. Angular Distributions of the Decay Radiation

Since the system which detects the light emanating from the interaction region is somewhat directional, one must consider processes which can cause a

magnetic-field-dependent angular distribution of this light.<sup>23</sup> At finite magnetic fields the  $\vec{L} \cdot \vec{S}$  interaction mixes the  $b$ ,  $c$ ,  $e$ , and  $f$  states in the high-field representation. Because the coefficients of the components are field dependent, the angular distribution of the 1215-Å light will, in general, be field dependent, whether one considers the decays  $4P-2S$  or  $4S-2P$ . Fortunately, the larger fraction of the rf-induced 1215-Å signal is due to a decrease in either the  $4\alpha$  or  $4\beta$  population, so that the application of a pertinent sum rule, which considers the decay to all  $2P$  sublevels, gives an angular distribution independent of field. Any of the four composite  $P$  states on the other hand is subject to this effect in decay to  $2S$ . A rough calculation shows that this “polarization asymmetry” will contribute at most 0.10 MHz to the  $\alpha c$  results for data normalized by the total light intensity. The three other transitions studied would be affected by less than this amount. This asymmetry, however, is eliminated for rf-normalized data when overlapping signals are negligible. A more exact correction for this phenomenon would be difficult to carry out since the angle of acceptance of the ellipsoidal light pipe is not well known.

#### F. Effect of the rf Field on the Electron Beam and Unpredicted Signals

A test was conducted to determine whether the modulated rf electric field could produce a signal when none was expected. If such an unexpected signal varied with magnetic field, then the data would contain an asymmetry unaccounted for in the line-shape fitting function.

To search for such an effect, the bombarding voltage (Fig. 7) was reduced below the He<sup>+</sup>,  $n = 4$  threshold value 75.6 V to about 68 V. The gun current was set to 2.2 mA, the helium pressure to 9.2 mTorr, and the microwave frequency to 16.030 GHz. The rf power level chosen was 200 mW, which was exceeded only in the  $S_4$  investigations, and then for a small number of runs. The signal detected around 3425 G under this set of operating characteristics was at most 1 part in 1400 of the  $\beta d$  resonance amplitude taken under the same conditions. The cause of such a signal might be due to the distant electron cyclotron resonance, to some complicated interaction between the rf electric field and the plasmlike environment existing in the interaction volume, to a resonance in the molecular-hydrogen impurity, to a resonance in the helium atom or to the “tail” of some resonance shown in Figs. 10 and 11. The location of the electron cyclotron resonance (indicated in Fig. 4) had a strong *a priori* influence on the final selection of data-taking regions. All the transitions investigated were many of their linewidths away from it. Since the size of this undesired signal was so small, its effect was ignored

in all the data analyses.

#### G. Additional Corrections to Data

In addition to the previously cited sources of error, four additional effects were considered. They are (i) corrections to the Zeeman theory, (ii) Bloch-Siegert shift,<sup>29</sup> (iii) Doppler shift, and (iv) spatial variation of the rf electric field amplitude.<sup>30</sup>

There are three known corrections to the particular form of the Zeeman theory used in the data analysis: (a) a relativistic effect, (b) an effect due to the motion of the nucleus, and (c) the effect of neglecting the term quadratic in the vector potential  $\vec{A}$ . Only the second cause has importance in the present work and it is easily accounted for by changing the value of  $g_L$  in the Hamiltonians from unity to  $1 - m/M$ , where  $m$  is the mass of the electron and  $M$  the mass of the nucleus.

The Bloch-Siegert shift can be loosely interpreted as an rf Stark shift of the atomic energy levels. The appropriate analysis predicts that the resonant circular frequency  $\omega$  should change in the presence of a microwave field such that

$$\omega \rightarrow \omega + V^2/4\nu ,$$

where  $V$  is the amplitude of the rf perturbation as used in Eq. (2) and  $\nu$  is the applied radio frequency. This shift is only 0.05 MHz for the highest-rf power level used in the  $\Delta E_4 - S_4$  studies. It was somewhat higher in the  $S_4$  investigations but still negligible with respect to the low-rf power effect discussed in Sec. IV C.

Since the ions in the experiment can have velocity components parallel to the waveguide axis, they experience a Doppler-shifted microwave frequency. For  $\nu = 16$  GHz, the Doppler shift is 0.07 MHz, assuming  $v = 1.39 \times 10^5$  cm/sec in the direction of microwave propagation. Since the ions in the experiment should be able to move in both directions perpendicular to the magnetic field with equal probabilities, this effect does not shift a resonance center, but rather, broadens the line symmetrically. The short at the end of the waveguide section shown in Fig. 9 reflects the microwaves incident on it and this aids in diminishing the effect of Doppler shifts. Specifically, if the ions travelled unidirectionally along the waveguide axis, they would experience the effect of two waves of nearly equal intensity propagating in opposite directions within the waveguide with frequencies located symmetrically on either side of the applied frequency. In this case, there would be no significant shift in the resonance center. Thus, depending on the quality of the short, one would expect a resultant shift of the resonance center to vary from about 0 to 0.07 MHz. In any case, error due to the Doppler effect in this experiment is not serious.

Finally, we consider the effect of the spatial vari-

ation of the rf electric field amplitude  $E$ , appearing in Eq. (3), across the 1-cm length of the interaction region. For resonances with little or no overlapping signals, as in the high-frequency measurements, the net result of such a varying field amplitude is to broaden the main resonance symmetrically and not change the location of its center. A shift will occur, however, if an overlapping resonance is not properly accounted for in the line shape. In the case of slight overlap, one is justified in ignoring these spatial variations since they are only adjustments to small corrections. The complications increase for resonances having more significant overlap problems, as in the  $S_4$  studies. We note, however, that the omission of such a consideration from the data analysis could not account for the pronounced break shown in Fig. 22. This is so because the unexplained changes in the  $S_4$  values occur when the microwave power is small. Thus, one can remove a common and hence unimportant factor  $E^2$  from the numerator of all the Lorentzian expressions describing the total signal.

## V. CONCLUSIONS

### A. $S_4$ Results

The  $\alpha e$  and  $\beta e$  resonances, which determine  $S_4$ , were each studied at two different microwave frequencies as shown in Fig. 11. For a fixed frequency, the gun current and pressure were systematically varied in the data taking. Under a given set of these three conditions, data were taken for many values of the rf power. The results of *all* such investigations revealed the same sort of pronounced break at low rf power portrayed in Fig. 22. The change in the  $S_4$  values for changes in the gun current was slight. However, variation of the pressure caused the results in Fig. 22 to translate uniformly about 2 MHz in the vertical direction. The largest value of pressure used in the  $S_4$  studies was 19 mTorr. The  $\alpha e$  results shown in this figure were approximately the lower limit of the  $(S_4)_{\text{experimental}} - (S_4)_{\text{theoretical}}$  discrepancy. Some  $\beta e$  studies at  $\nu = 9630$  MHz and for other values of helium pressure and gun current had discrepancies somewhat larger than those depicted.

In spite of this unaccountable rf power effect, it is felt that the investigation allows for a direct determination of  $S_4$  to an accuracy of  $\pm 5$  MHz. This error limit is chosen to encompass all the  $\alpha e$  and the vast majority of the  $\beta e$  results when the experimental value of  $S_4$  is taken approximately equal to its theoretical value. In this way, one obtains

$$S_4 = 1768 \pm 5 \text{ MHz} ,$$

where the indicated uncertainty is meant to represent a 68% confidence level.

B.  $\Delta E_4 - S_4$  Results

A regression analysis of the high-frequency results was conducted to account for the observed dependence of the  $\Delta E_4 - S_4$  resonance centers on the excitation current and pressure. Though the collisional-quenching analysis outlined in Sec. IV B could roughly account for these dependences, it was felt that the approximations involved in that development unduly restricted one's confidence in the final results. Instead, a straightforward extrapolation of the  $\alpha c$  and  $\beta d$  centers was made to zero values of current and pressure. The extrapolation of the high-frequency resonance centers included an  $IP$  and a  $P$  term for the reasons given in Sec. IV B. If one defines a quantity  $\Delta$  such that

$$\Delta = (\Delta E_4 - S_4)_{\text{experimental}} - (\Delta E_4 - S_4)_{\text{theoretical}},$$

then the fitting function in the regression analysis becomes

$$\Delta_{\text{raw}} = \Delta_0 + C_1 IP + C_2 P,$$

where  $\Delta_{\text{raw}}$  is obtained from data analysis in which the line shape is a sum of two terms like that in Eq. (3), i. e., one for the  $\alpha c$  resonance and one for the  $\beta d$  resonance;  $\Delta_0$ ,  $C_1$ , and  $C_2$  are fitted constants. The factor  $\omega - \nu$  in the resonance denominator of Eq. (3) can be written as

$$\omega - \nu = [\omega(H) + \Delta_{\text{raw}}] - \nu,$$

in which  $\omega(H)$  depends on an assumed value for  $\Delta E_4 - S_4$  and  $\Delta_{\text{raw}}$  is the corresponding experimentally determined correction to this value.

Only the results of the three-point data-taking method described in Sec. III C were used in obtaining a final value for  $\Delta E_4 - S_4$ . The multipoint pan-

oramics were analyzed to verify that the line shape chosen for the fitting program had no abnormalities which would go unnoticed in the three-point data analysis. In all, 136  $\alpha c$  runs taken at a microwave frequency of 16.030 000 GHz and 73 runs taken at 17.030 000 GHz along with 148  $\beta d$  runs taken at 16.030 000 GHz were involved in the final evaluation of  $\Delta E_4 - S_4$ . Data on  $\beta d$  were taken at the second frequency, but not included in the final evaluation because the increased quenching effectiveness of the  $\beta f$  crossing would require the extrapolation to account for a several megahertz dependence of  $\Delta_{\text{raw}}$  on the gun current and pressure. Each run provided data for three different analyses: one for the low-rf normalized signal, a second for the high-rf normalized signal, and a third for the rf-normalized signal. Table II summarizes the results of these investigations. All the runs listed here were taken with the cathode at a potential -400 V below that of the grounded grid and anode. The bombarding voltage has been reduced to 250 V for some runs; but only a negligible change from the 400 V results was found. The values of the fitted constants  $C_1$  and  $C_2$  are tabulated in Ref. 30, p. 102. Typically,  $C_1$  was 0.05 MHz/(mA mTorr), while  $C_2$  was around 0.1 MHz/mTorr. The values of  $\Delta_0$  listed in the first column of Table II had error assignments from the regression analysis which were based on standard deviations of the mean ( $\sigma$ ) obtained from several three-point runs taken under a fixed set of experimental conditions. The analysis used a weighting factor  $1/\sigma^2$ . Successive columns in Table II list the relevant corrections and uncertainties. The last column of  $\Delta_0$  values presents the final corrections to  $(\Delta E_4 - S_4)_{\text{theoretical}}$  which yield the experimental re-

TABLE II. Regression results, final corrections, and uncertainties for  $\Delta_0$ .

	$\Delta_0^a$ (with NMR correction) (MHz)	Stark effect and its uncertainty <sup>b</sup> (MHz)	NMR-correction uncertainty <sup>c</sup> (MHz)	Overlap-correction uncertainty <sup>d</sup> (MHz)	Final values for $\Delta_0^e$ (MHz)
<i><math>\alpha c</math> results</i>					
<i>L</i> <sup>f</sup>	-2.64 ± 0.42	+0.14 ± 0.05	± 0.05	± 0.10	-2.50 ± 0.44
<i>H</i>	-2.93 ± 0.65	+0.14 ± 0.05	± 0.05	± 0.10	-2.79 ± 0.66
<i>RF</i> <sup>g</sup>	+1.10 ± 1.21	+0.14 ± 0.07	± 0.07	± 0.14	+1.24 ± 1.22
<i><math>\beta d</math> results</i>					
<i>L</i>	-0.16 ± 0.33	-0.10 ± 0.03	± 0.05	± 0.10	-0.26 ± 0.35
<i>H</i>	+0.15 ± 0.26	-0.10 ± 0.03	± 0.05	± 0.10	+0.05 ± 0.29
<i>RF</i>	-2.07 ± 0.64	-0.10 ± 0.04	± 0.07	± 0.14	-2.17 ± 0.66

<sup>a</sup>In determining  $\Delta_{\text{raw}}$ , and therefore  $\Delta_0$ , the value  $(\Delta E_4 - S_4)_{\text{theoretical}} = 20\,180.78$  MHz cited in Ref. 2 was used.

<sup>b</sup>Uncertainty is taken to be one-third of the correction.

<sup>c</sup>The *correction* for some runs was as much as 0.48 MHz and 1.10 MHz for the low- and high- frequency transitions, respectively.

<sup>d</sup>Upper limit.

<sup>e</sup>Error designations in this column are the root-sum-squares of the ones given horizontally.

<sup>f</sup>*L*, *H*, and *RF* labels represent the results for the low, high, and rf normalization procedures.

<sup>g</sup>*RF* uncertainties in columns 2-4 are obtained by multiplying those for *L* and *H* by  $\sqrt{2}$ .

sult for the  $4^2S_{1/2}-4^2P_{3/2}$  energy separation.

Three immediate observations are made on the final  $\Delta_0$  values from Table II: (a) For a given transition, the results that depend on normalization by the total light intensity, i. e.,  $L$  and  $H$ , agree quite well. (b) For a given transition, the  $L$  and  $H$  results disagree markedly with those obtained by the rf-normalization technique. (c) In a comparison of the  $L$  or  $H$  results against those labeled  $RF$ , the results for the two transitions "reverse" themselves. One may offer at least three explanations for this behavior in  $\Delta_0$ . (i) There are certain unaccounted-for systematic effects involved. (ii) The estimated values for the indicated systematic effects were made too small. (iii) Finally, these results are within the outer limits of statistical variation. Only the first alternative seems reasonable.

The final results for  $\Delta_0$  given in Table II will be used in the following way.

(a) Since for a given transition, the  $L$  and  $H$  results agree so well, they will be combined via the method of weighted averages, where the weighting will be equal to  $1/\sigma^2$ , to obtain a single result per transition for data normalized by the total light intensity.

(b) The remaining four values for  $\Delta_0$  will be combined in pairs, first for each transition and then for each normalization scheme, where the method of combination will use the errors given in Table II added quadratically to the unknown systematic error which will be taken equal to the rms deviation of the two selected results for  $\Delta_0$  from their average value.

(c) These values will then be combined by the weighted-average method to produce two penultimate results for  $\Delta_0$ .

Following this procedure, one obtains the two results for  $\Delta_0$  of  $-1.03 \pm 1.11$  MHz and  $-1.12 \pm 1.14$  MHz considering first the separate transitions  $\alpha c$  and  $\beta d$  and then the two normalization schemes used in studying these transitions. Since each of these quantities is on equal footing, a final  $\Delta_0$  value is obtained by taking the midpoint of the extreme

limits of these values considered together yielding

$$\Delta_0(\text{final}) = -1.1 \pm 1.2 \text{ MHz} .$$

We thus obtain

$$(\Delta E_4 - s_4)_{\text{experimental}} = 20179.7 \pm 1.2 \text{ MHz} ,$$

where the error is meant to indicate a 68% level of confidence that this final result will agree with the "true" value.

If one subtracts this quantity from the theoretical value of  $\Delta E_4$  given in Table I, one obtains an *indirect* experimental value for the level shift  $s_4$ , i. e.,

$$(s_4)_{\text{experimental}} = 1769.4 \pm 1.2 \text{ MHz} .$$

Again, with the aid of Table I, one obtains the difference

$$(s_4)_{\text{experimental}} - (s_4)_{\text{theoretical}} = +1.1 \pm 1.3 \text{ MHz} ,$$

which implies no conflict with the prediction of quantum electrodynamic theory to this level of accuracy. Indeed, if the new theoretical result for  $s_4$  reported by Appelquist and Brodsky<sup>3</sup> is taken, the difference  $(s_4)_{\text{experimental}} - (s_4)_{\text{theoretical}}$  is reduced to  $(+0.4 \pm 1.3)$  MHz.

In conclusion, we note that the values for the fine-structure separations in  $\text{He}^+$  presented in this paper, i. e.,

$$s_4 = (1768 \pm 5) \text{ MHz (see Ref. 31) ,}$$

$$\Delta E_4 - s_4 = (20179.7 \pm 1.2) \text{ MHz} ,$$

are to be compared with the heretofore most accurate determinations  $s_4 = 1766.0 \pm 7.5$  MHz (see Ref. 9) and  $\Delta E_4 - s_4 = 20180 \pm 2$  MHz (see Ref. 32).

#### ACKNOWLEDGMENTS

We gratefully acknowledge the assistance given by Dr. D. L. Mader, Dr. S. L. Kaufman, Dr. W. H. Wing, and Dr. M. Leventhal in several stages of the research. The services of the Physics Department Electronics Shop headed by R. J. Blume, and the construction skills of the Physics Department Machine Shop under the supervision of A. Disco, also contributed valuably.

\*Research supported in part by the U. S. Air Force Office of Scientific Research. Paper based in part on material submitted by Ralph R. Jacobs in partial fulfillment of the requirements for the degree of Doctor of Philosophy at Yale University.

<sup>1</sup>Present address: General Telephone and Electronics Laboratories, Bayside, N. Y.

<sup>2</sup>W. E. Lamb, Jr. and R. C. Retherford, *Phys. Rev.* **72**, 241 (1947).

<sup>3</sup>B. N. Taylor, W. H. Parker, and D. N. Langenberg, *Rev. Mod. Phys.* **41**, 375 (1969). A convenient listing of all the experimental and theoretical fine-structure values for hydrogenic atoms is included in this paper. We have chosen to use three standard deviations for the theoretical uncertainty in both  $s$  and  $\Delta E - s$  in our paper.

<sup>4</sup>Many people have contributed to the calculation of  $s_n$  and  $\Delta E_n$  for one-electron atoms. A summary of the theoretical efforts is presented in G. W. Erickson and D. R. Yennie, *Ann. Phys. (N. Y.)* **35**, 271 (1965); **35**, 447 (1965). Reference 2 (above) evaluates these intervals for  $\alpha^{-1} = 137.03602(21)$ . A new calculation of  $s_n$  has recently been made by T. Appelquist and S. J. Brodsky, *Phys. Rev. Letters*, **24**, 562 (1970).

<sup>5</sup>G. W. Series, *Proc. Roy. Soc. (London)* **A226**, 377 (1954).

<sup>6</sup>G. Herzberg, *Z. Physik* **146**, 269 (1956).

<sup>7</sup>F. L. Roesler and L. DeNoyer, *Phys. Rev. Letters* **12**, 396 (1964).

<sup>8</sup>F. L. Roesler and J. E. Mack, *Phys. Rev.* **135**, A58 (1964).

<sup>8</sup>H. P. Larson and R. W. Stanley, *J. Opt. Soc. Am.* **57**, 1939 (1967).

<sup>9</sup>L. L. Hatfield and R. H. Hughes, *Phys. Rev.* **156**, 102 (1967).

<sup>10</sup>H. J. Beyer and H. Kleinpoppen, *Z. Physik* **206**, 177 (1967).

<sup>11</sup>K. R. Lea, M. Leventhal, and W. E. Lamb, Jr., *Phys. Rev. Letters* **16**, 163 (1966). The present paper continues the work described in this reference.

<sup>12</sup>T. G. Eck and R. J. Huff, *Phys. Rev. Letters* **22**, 319 (1969); and R. J. Huff, thesis, Case Western Reserve University, 1969 (unpublished).

<sup>13</sup>T. Hadeishi, *Phys. Rev. Letters* **21**, 957 (1968); **22**, 815 (1969).

<sup>14</sup>G. W. Series and W. N. Fox, *J. Phys. Radium* **19**, 850 (1958).

<sup>15</sup>G. W. Series, *Phys. Rev.* **136**, A684 (1964).

<sup>16</sup>Reference 5 gives the lifetimes for the n = 4 levels in units of 10<sup>-8</sup> sec: 4S, 1.4154; 4P, 0.07687; 4D, 0.2258; 4F, 0.4531. We adopt the following convention: When a symbol like  $\nu$ ,  $\omega$ ,  $\gamma$ , or  $V$  is inserted in a formula such as Eq. (3), it should be expressed in circular frequency units of sec<sup>-1</sup>. In other places, the corresponding numerical value is given in ordinary frequency units, e.g.,  $\$4 = 1768$  MHz or  $\nu = 16.030$  GHz.

<sup>17</sup>W. E. Lamb, Jr. and T. M. Sanders, Jr., *Phys. Rev.* **119**, 1901 (1960).

<sup>18</sup>L. R. Wilcox and W. E. Lamb, Jr., *Phys. Rev.* **119**, 1915 (1960).

<sup>19</sup>The early papers on hydrogen fine structure are referred to as HI through HVI: HI, W. E. Lamb, Jr. and R. C. Retherford, *Phys. Rev.* **79**, 549 (1950); H II, **81**, 222 (1951); H III, W. E. Lamb, Jr., *ibid.* **85**, 259 (1952); H IV, W. E. Lamb, Jr. and R. C. Retherford, *ibid.* **86**, 1014 (1952); H V, S. Triebwasser, E. S. Dayhoff, and W. E. Lamb, Jr., *ibid.* **89**, 98 (1953); H VI, E. S. Dayhoff, S. Triebwasser, and W. E. Lamb, Jr., *ibid.* **89**, 106 (1953).

<sup>20</sup>*Mathematical Methods for Digital Computers*, edited by A. Ralston and H. S. Wilf (Wiley, New York, 1960).

<sup>21</sup>W. E. Lamb, Jr. and M. Skinner, *Phys. Rev.* **78**,

539 (1950). These authors indicate how the 4S cross section should be calculated. The cross sections for the 4P, 4D, and 4F states are the products of the corresponding atomic-excitation cross sections [cf. H. S. W. Massey, in *Encyclopedia of Physics*, edited by S. Flügge (Springer, Berlin, 1956), Vol. XXXVI, p. 360] and the sudden-approximation result for the probability of ionization of the inner electron.

<sup>22</sup>W. L. Wiese, M. W. Smith, and B. M. Glennon, *Atomic Transition Probabilities* (Nat. Bur. Std., U. S. GPO Washington, D. C., 1966), Vol. I.

<sup>23</sup>S. L. Kaufman, W. E. Lamb, Jr., K. R. Lea, and M. Leventhal, *Phys. Rev. Letters* **22**, 507 (1969); and (unpublished).

<sup>24</sup>E. B. D. Lambe, thesis, Princeton University, 1959 (unpublished).

<sup>25</sup>D. J. T. Morrison and M. R. H. Rudge, *Proc. Phys. Soc. (London)* **89**, 45 (1966). This paper supports a result of the sudden approximation treatment — that the excitation cross sections vary roughly as 1/n<sup>3</sup> for increasing n.

<sup>26</sup>R. M. St. John and C. C. Lin, *J. Chem. Phys.* **41**, 195 (1964).

<sup>27</sup>Similar total light intensities below the helium-ion excitation thresholds were seen in three other fine-structure investigations: R. Novick, E. Lipworth, and P. F. Yergin, *Phys. Rev.* **100**, 1153 (1955), on He<sup>+</sup>, n = 2; E. Lipworth and R. Novick, *ibid.* **108**, 1434 (1957), on He<sup>+</sup>, n = 2; and D. Mader (private communication) on He<sup>+</sup>, n = 3.

<sup>28</sup>E. M. Purcell, *Astrophys. J.* **116**, A57 (1952); M. J. Seaton, *Proc. Phys. Soc. (London)* **68**, 457 (1954). A more detailed presentation of the collisional quenching effects discussed in this section can be found in Ref. 30.

<sup>29</sup>The first two sources of error are discussed in H III (Ref. 19).

<sup>30</sup>All four corrections are more fully dealt with in R. R. Jacobs, Ph.D. thesis, Yale University, 1969 (unpublished).

<sup>31</sup>R. R. Jacobs, K. R. Lea, and W. E. Lamb, Jr., *Bull. Am. Phys. Soc.* **14**, 942 (1969).

<sup>32</sup>R. R. Jacobs, K. R. Lea, and W. E. Lamb, Jr., *Bull. Am. Phys. Soc.* **14**, 525 (1969).

## Experimental Determination of Relative Radiative Decay Rates of Vacancies in the K Shell\*

A. G. de Pinho

*Department of Physics, Pontifícia Universidade Católica, Rio de Janeiro ZC-20, Brasil*

(Received 31 August 1970)

A high-resolution Ge(Li) x-ray spectrometer was used for measuring relative radiative decay rates of vacancies in the K shell of the following atoms: Au, Hg, Tl, Pb, Bi, Rn, Ra, Th, and U. In the most favorable cases, the x rays following the filling of a K vacancy by L<sub>II</sub>, L<sub>III</sub>, M<sub>II</sub>, M<sub>III</sub>, M<sub>IV</sub>, M<sub>V</sub>, N<sub>II</sub>, N<sub>III</sub>, N<sub>IV-V</sub>, and O<sub>II-III</sub> electrons were observed and measured. The results were compared with recent relativistic calculations carried out by Scofield.

### I. INTRODUCTION

The use of silicon- and/or germanium-lithium-drifted detectors is giving a new impulse to x-ray spectrometry. The very good resolutions that can

be attained, the high peak-to-Compton ratios, and the possibility of obtaining very accurate efficiency-vs-energy curves render this instrument comparable or even superior to the traditional x-ray spectrometers, viz., bent-crystal systems and ioniza-